STUDY AND CHARACTERIZATION OF A NOVEL SMALL HEAT SHOCK PROTEIN FROM *BABESIA*

A Dissertation

by

KENNETH HARRIS CARSON

Submitted to the Office of Graduate Studies of
Texas A&M University
in partial fulfillment of the requirements for the degree of

DOCTOR OF PHILOSOPHY

August 2006

Major Subject: Medical Sciences

STUDY AND CHARACTERIZATION OF A NOVEL SMALL HEAT SHOCK PROTEIN FROM *BABESIA*

A Dissertation

by

KENNETH HARRIS CARSON

Submitted to the Office of Graduate Studies of
Texas A&M University
in partial fulfillment of the requirements for the degree of

DOCTOR OF PHILOSOPHY

Approved by:

Chair of Committee,	Allison C. Rice-Ficht
Committee Members,	J. Martin Scholtz
	C. Nick Pace
	Thomas Ficht
Head of Department,	J. Martin Scholtz

August 2006

Major Subject: Medical Sciences

ABSTRACT

Study and Characterization of a Novel Small Heat Shock Protein from *Babesia.*

(August 2006)

Kenneth Harris Carson, B.S., The University of Texas at Tyler

Chair of Advisory Committee: Dr. Allison C. Rice-Ficht

Many proteins can easily attain a non-native fold and be of no use or even a detriment to the host. The host cell has a myriad of molecules dedicated to assisting nascent and existing proteins in folding properly and maintaining the native fold. Of these molecular chaperones, the small Heat Shock Proteins (sHSP's) are an important group and worthy of study. The sHSP's are a diverse group of proteins that have in common an α-crystallin domain and generally display a chaperone activity. A sHSP (HSP20) isolated from the cattle parasite *Babesia bovis* has similar activities, and limited sequence homology to other α-crystallins. The gene encoding HSP20 was cloned into an expression system where the gene product was induced and purified for study. It was shown that HSP20 inhibits thermally induced aggregation of alcohol dehydrogenase at equimolar ratios. HSP20 was also used to significantly reduce amyloid formation of the β-Amyloid (1-40) Peptide *in vitro* at the sub-stoichiometric ratio of 1:10. A study of the oligomeric forms of HSP20 using size exclusion chromatography and gel electrophoresis revealed a broad range of multimers present in solution. The distribution of oligomers was affected by altering the solution conditions and concentration of the protein. The domains responsible for multimerization of HSP20 were mapped via sequence

homology with known α-crystallins. These regions correspond to 12 carboxy-terminal amino acids and 50 amino-terminal amino acids. Truncated versions of HSP20 lacking these proposed oligomerization domains were created using PCR of the original gene and cloning into an expression vector as before. Using size exclusion chromatography, gel electrophoresis and analytical centrifugation, we show that the deleted domains alter the multimeric population of the protein in solution. The carboxy-terminal domain has a slight effect on multimerization while the amino-terminal deletion results in a drastic reduction in any multimers above a dimer under the conditions tested. Despite this drastic change in the multimerization of HSP20, there were no changes in the activities observed when compared to the full-length form. From this we conclude that the regions responsible for multimerization play little role in the observed activities of HSP20.

DEDICATION

To my parents who taught me to dream and set goals

To my teachers who gave me the tools to achieve those goals

To my daughter, McKenna who taught me joy

To my wife, Tammi who taught me how to live and love

ACKNOWLEDGEMENTS

I would like to thank my advisor and mentor Dr. Allison C. Rice-Ficht for her help and support. I would like to thank my committee members Dr. Pace, Dr. Scholtz and Dr. Thomas Ficht for their advice and council. I also thank Dr. Barbara J. Ruef for her training and advice in my early days in the lab as well as for developing the original HSP20 clone and polyclonal antiserum against the protein. I thank my lab mates for their patience and help over the years. I must thank my family for the support and patience they have extended to me over these past years. I thank my wife, Tammi for letting me pursue this goal and having infinite patience with me. Maniac honks entrance lovers most.

TABLE OF CONTENTS

LIST OF FIGURES

FIGURE Page

LIST OF TABLES

CHAPTER I

INTRODUCTION

The ability of a protein to attain a native or active folded state is not a trivial one. The process by which a protein folds into its native form is crucial, but often is not spontaneous. Molecular crowding, salt concentrations, reducing and oxidizing conditions and the high concentration of other proteins may all contribute to a protein folding incorrectly (Figure 1). Non-native forms of a protein are often stabilized by interactions between partially folded intermediates and other molecules. Regions of a protein made accessible when in the non-native form could also lead to the stabilization of an inactive form. In some cases, an amyloidogenic form of a protein is stabilized. This leads to amyloid fibril formation which involves the conversion of a normally soluble protein or peptide into an insoluble aggregate high in beta sheet structure (Figure 1).

Proteins that are not folded correctly do not perform their functions properly. They may even be detrimental to the health of the host organism and must be disposed of by the cell. Therefore, the cell has devised ways to combat the tendency of proteins to fold improperly. Molecular chaperones are required in many cases to ensure the proper folding of proteins (*1*).

The term "molecular chaperone" describes a wide range of molecules recruited by the host cell to assist in the proper folding of nascent and existing proteins.

This dissertation follows the style of *Biochemistry.*

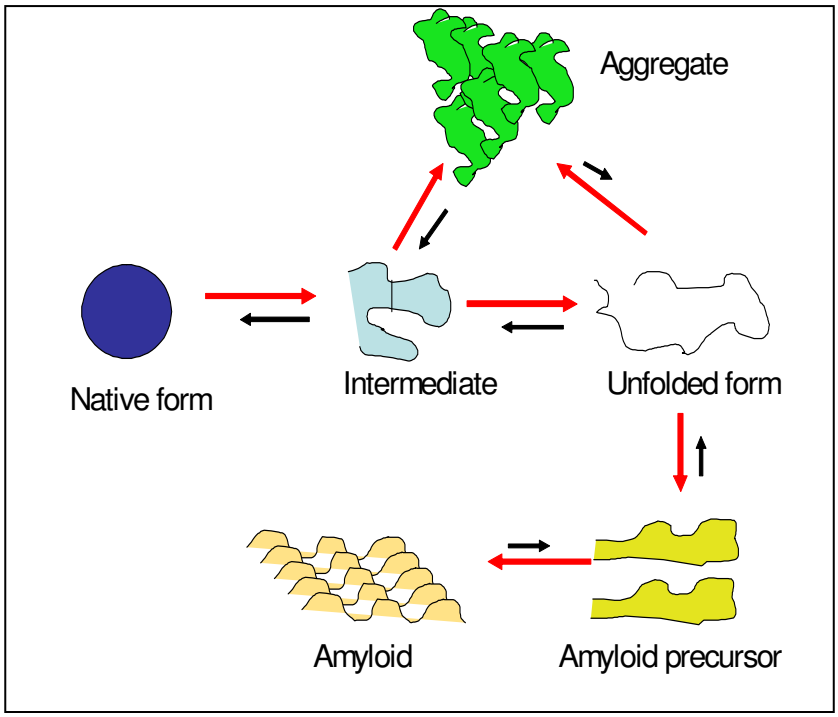

Figure 1 Overview of possible native and non-native protein states in the cell. Native proteins are in equilibrium with unfolded intermediates. Under certain conditions, those intermediate forms are stabilized leading to interactions between regions of the protein not normally accessible. This could result in aggregation. An amyloidogenic form of the protein could also be stabilized leading to amyloid fibril formation

This very important class of molecules has been shown to assist in protein folding, translocation and assembly of active protein complexes within cells.

An Overview of Molecular Chaperones

As nascent chains are translated, they are not allowed to fold due to the confined space of the ribosome. Also, many native folds cannot be attained until a large majority or the entire protein is translated. During this time, many regions of the protein are exposed to an environment that could lead to stabilization of a non-native folded form of

the protein (misfolding). This propensity to misfold is often exacerbated by other nascent chains being translated at the same time and in very close proximity that are themselves partially or completely unfolded (*2*). Both prokaryotes and eukaryotes have chaperones to assist nascent chains with proper folding. In prokaryotes, proteins needing assistance in folding often interact with dnaJ and dnaK. Proper folding is attained by a series of ATP-dependent bindings and dissociations. If additional folding is needed, the nascent protein can interact with GroEL and GroES. Here, the nascent chain is enclosed by the chaperones and sequestered from other molecules while it attains the native fold. Again, ATP is needed to enclose the protein within the "shell" of chaperones (*2*). A similar system is in place in eukaryotes (TRiC). Here, the nascent chain interacts with HSP-40, -70, and -90 (as proteins interact with dnaJ and K in prokaryotes) as it is translated from the ribosome. TRiC is a complex similar to that of GroEL and GroES allowing the protein to fold in a protected environment (*2*).

Many chaperones are constitutively expressed; however, the environment of a cell can change causing stress. During times of physiologic stress on an organism, some chaperones are upregulated. This group of chaperones is known as the Heat Shock Proteins (HSP). Members of this large group of proteins are upregulated by the host in response to various stresses such as temperature change, pH, and oxidative stress. The family of chaperones known as small Heat Shock Proteins (sHSP's) are a large and functionally diverse group that are the subject of a great deal of study (*3*).

The sHSP's are a large set of chaperones ranging from 12 to 43 kDa in size. They are phylogenetically diverse and are active in many areas of the cell (*2*). These

molecules assist in maintaining the native folds of proteins in an ATP-independent manner until other chaperone machinery can refold the proteins. These sHSP's typically have the ability to assemble into dynamic oligomers ranging in size form 300 kDa to 1 MDa and above (*4, 5*). The chaperone activity generally requires a disassembly of these large multimeric complexes (*2*). However, it is not completely clear what role, if any, the multimerization of the sHSP's plays in their activity.

The major structural motif of the sHSP's is the α-crystallin domain. This ~95 amino acid region is characterized by many β-strands arranged in a β sandwich that is thought to be the primary site of interaction with unfolded proteins. It is also thought to be responsible for dimer formation. An amino terminal region, often unstructured and of variable length, is thought to be responsible for higher-order structures and modulation of some chaperone activity. A carboxy-terminal region (about 12 amino acids in length) is thought to be responsible for interactions between smaller multimers leading to assemblies larger than dimers as well as modulation of chaperone activity (*5, 6*). Multimeric assembly and chaperone activity appear to be linked as the multimeric state of the protein seems to vary with temperature (*1, 2, 4-9*). Thus, affecting the multimeric assembly may by default affect the chaperone activity.

The main structural motif of the sHSP's is the α-crystallin domain. The term "crystallin" refers to the major structural proteins in the eye lens of vertebrates that are responsible for its refractive power (*10*). The crystallins make up over 90% of the total mass of the lens. Of these proteins, approximately one-third is alpha-crystallin. There are two forms of the protein that are closely related and share a high degree of sequence

homology: αA- and αB-crystallin. The remaining two-thirds are two related crystallins: β and γ. These proteins form an oligomeric distribution in solution typically ranging in size from 300 kDa to over 1 MDa, while the molecular weight of the monomeric protein is about 20 kDa (*10*). Circular dichroism spectroscopy (CD) studies predict the beta-pleated sheet form dominates the secondary structure of the α-crystallins (*6, 9-11*).

Crystallins have been found in many other cells of the human body (as well as other organisms) though never in concentrations approaching that found in the lens of the eye (*10*). The presence of α-crystallins in the lens lead to research of the proteins' function *in vivo* (*10-12*). Horwitz and others concluded that the protein plays a vital role in the continued clarity of the lens. The subsequent clouding and cataract formation in older patients is attributed to decreasing α-crystallin activity with age. Indeed, mutations in α-crystallin result in cataract formation early in the patient's life (*6, 10*). This is compelling evidence that the function of the protein in the lens is to keep other proteins from aggregating. A point mutation (R120G) in α-B-crystallin results in loss of function of the gene product. The molecular weight of the oligomer of the mutant is very different from wild type (*10*). While wild type α-B-crystallin has a multimeric molecular weight of approximately 540 kDa, the (R120G) mutant forms much more irregularly-shaped assemblies with an average molecular weight of about 850 kDa (*10*). Patients with this mutation suffer from Desmin-related myopathies (DRM) which are characterized by accumulation of aggregates of desmin. Patients suffer from various muscle problems as well as the development of cataracts. Many crystallins share homology with small heat-

shock proteins. α-Crystallin has been implicated in the survival of cells subjected to heat shock or oxidative stresses by conferring increased stability on actin fibers (*8*).

Several sHSP's have been studied. Kim et al. have performed extensive studies on a sHSP from the hyperthermophilic archeon *Methanococcus jannaschii* designated HSP 16.5 (*13-17*). van Montfort et al. studied a sHSP from wheat termed 16.9 (*6*). Both of these proteins have been crystallized and models of their multimeric assembly have been proposed (*6, 14, 16*). Unlike other α-crystallins, these proteins seem to have a more distinct multimeric structure, thus facilitating their crystallization.

Horwitz was one of the first to show that α-crystallin acted as a molecular chaperone (*10, 11*). He showed that α-crystallin purified from the lenses of bovine eyes was as effective as GroEL in suppression of aggregation of α-glucosidase at elevated temperature (*11*). Horwitz went on to show that α-crystallin could inhibit aggregation of several enzymes including glutathione S-transferase, citrate synthase and horse liver alcohol dehydrogenase at elevated temperatures (*11*). The suppression of aggregation of other important lens proteins (β-crystallin) by α-crystallin was also shown by Horwitz (*11*). The two forms of the chaperone (αA- and αB-crystallin) were both effective in preventing thermal aggregation of the substrates tested. It is important to note, that this inhibition of aggregation (measured by apparent light scattering) required stoichiometric amounts of the chaperone though it was (and still is) thought to exist as a large multimer. Horwitz concludes his early work with a discussion on the need to know and understand the active form of the chaperone (*11*). This is still a subject of much debate as more sHSP's are being discovered with different multimeric assemblies.

The 16.5 kDa sHSP from *M. jannaschii* shares 20.7% sequence identity with human αA-crystallin and 31.4% identity with a rice sHSP (HSP16.9). However, unlike other sHSP's that form a population range of multimeric species in solution, *M. jannaschii* HSP16.5 forms a stable oligomer of 24 subunits. This structure is visible using electron microscopy and is approximately 15-20 nm in diameter (*9*). Kim showed that the protein could be used to stabilize a wide range of proteins against thermal degradation. It is important to note that the researchers observed a substrate-dependent range of molar ratios of substrate to sHSP in order to inhibit aggregation. This was thought to be a result of the different temperatures at which the substrate began to denature and the subsequent activity of the sHSP at that temperature (*9*).

The proposed structure of *M. jannaschii* HSP16.5 is a hollow spherical complex of 24 monomers. The α-crystallin domain of each monomer forms a β sandwich that incorporates one of the strands from a neighboring molecule creating a dimer. The structure has several holes or "windows" opening to a core (*14*). The amino termini of all monomers are highly disordered while the carboxy terminus of each monomer is highly ordered. The crystal structure reveals many points of contact between interacting monomers with hydrogen bonds, ionic and hydrophobic interactions all playing roles in the assembly of the oligomer (*14*). Because of the location of these contacts, it was theorized that the dimer is the "building block of the sphere". The authors also concluded that the disordered amino termini were inside the sphere (*14*). They go on to conclude that the interior of the structure could be used to sequester RNA or proteins during times of environmental stress or the structure itself could simply be a storage

mechanism for the protein until the host is exposed to a stress and the protein becomes active (*14*). Later research by the same group showed that the secondary structure of the protein changes very little at high temperatures (80°C). It is at this high temperature that the protein interacts with the substrate single-chain monelin (*17*). Through a number of approaches, the researchers found that the substrate binds to the outside of the HSP 16.5 sphere and is thus not capable of forming aggregates with itself *in vitro*. Finally, it was found by Kim et al. that the unstructured amino region of the protein "had no structural role", but that it might play a role in the kinetics of oligomerization by acting as a nucleation site or condensing area for monomers (*17*).

A second sHSP from wheat (HSP 16.9) was crystallized by van Montfort et al (*6*). The quaternary structure is made up of two rings composed of 6 monomers each resulting in a dodecamer. Again, the dimer is a result of interactions between the α-crystallin domains of two monomers. The researchers were able to show through their crystal structure that the carboxy terminus appeared to be involved in interactions between sets of dimers on different disks in some cases and to dimers in the same disk at other times (*6*). The authors went on to show that the N-terminal regions are structured in half of the monomers. The structured arms from two adjacent hexameric disks interact with one another to form a helical domain on the inside of the dodecamer. This creates a more compact multimer and adds rigidity to the whole structure (*6*). The N- and C- termini were shown to be of great importance to oligomeric assembly of HSP 16.9. van Montfort et al show that the sHSP from wheat disassembles at higher temperatures as evidenced by size exclusion chromatography (*6*). Because of this

disassembly at elevated temperatures, van Montfort proposes that unfolded proteins interact with the α-crystallin domain of HSP16.9 in an active "subassembly" form.

At first glance, the two proteins discussed above have limited similarity. However, structurally they have some common features. The fold of the α-crystallin domain of wheat HSP16.9 is very similar to that reported for the *M. jannaschii* HSP16.5, though sequence homology is relatively low between the two proteins (*1, 6*). A common motif of IXI/V is seen in the C-terminal extensions of both proteins as well (*1, 6*). Another conserved residue found in HSP 16.9 is Arg 108. This residue is equivalent to residue 120 in human αA-crystallin. Arg107 is the equivalent residue in *M. jannaschii* (*1*). As stated earlier, mutations at this site in the human homolog causes an apparent loss of function. Finally, a conserved quaternary interaction involving the binding of the C-terminal region into a groove of the α-crystallin domain is seen in both crystal structures. Despite these structural similarities, the quaternary structure is quite different (*6*).

From all the research performed on sHSP's, many groups have proposed models of how these molecules function in the hierarchy of chaperones within the cell. Figure 2 illustrates a possible scheme of protection against unwanted aggregation and where the α-crystallin sHSP's might function within it. Here, the sHSP is represented as a multimer that acts as a sink for intermediate and unfolded forms of the protein. These proteins are not allowed to interact with other molecules that might lead to aggregation. Instead, they are sequestered from these undesirable interactions and are thus allowed to

return to their native form independently or with the assistance of the active refolders such as dnaK or GroEL.

An Overview of Amyloid Fibril Formation and the Amyloidoses

Though aggregation might often seem to be an unordered state of a protein, this is not always the case. A specialized form of protein aggregation seen in a group of

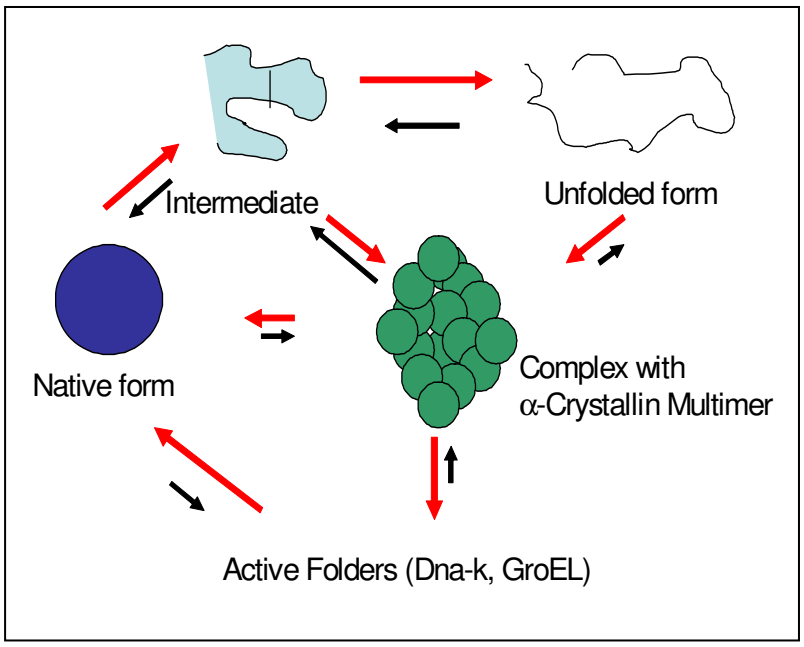

Figure 2 Possible role of α-crystallin in maintaining native protein folds. The crystallin is represented as a multimer. Unfolded and intermediate forms of the protein interact with regions of the crystallin multimer and are sequestered from other interactions that might lead to aggregation. The protein is then allowed to refold or is assisted by the active folders represented here by dnaK and GroEL

disorders is termed amyloid and is very highly ordered. Amyloid was first observed by Rudolph Virchow in 1854 through staining the cerebral copora amylacae with iodine. He noted a strange macroscopic appearance that stained blue. He concluded it to be starch and named it amyloid (from the Latin amylum meaning starch) (*18*). Later research sparked debate as to whether or not the deposits were fat or carbohydrate in nature. Finally, Friedreich and Kekule showed amyloid was in fact proteinaceous and contained no carbohydrate (*18*).

Researchers later utilized the amyloid-specific dye Congo red to identify amyloid. This planar aromatic dye shows altered spectroscopic properties when in the presence of amyloid. The birefringence observed when amyloid was stained with Congo red indicated an ordered structure and has since been adopted as a criterion of amyloid (*18*). Later, electron microscopic studies of amyloid tissues were performed. It was immediately recognized that many amyloid forms showed similar structure in tissues characterized by bundles of straight rigid fibrils. This structure became the second criterion for the definition of amyloid (*18*). The amyloid fold is characterized by monomers of beta strands oriented perpendicular to the axis of the fibril. It is these stacked beta strands that appear as rigid fibrils using electron microcopy (*18*).

There are several possible models for amyloid fiber formation. The simplest possible mechanism that explains fibril formation is the nucleation model (*19*). This model was chosen based on the observation of a lag phase in fibril development followed by a much more rapid elongation phase. This lag phase is reported to consist of a rate-limiting nucleation step that produces an organized amyloidogenic nucleus of

monomeric proteins/peptides (*19*). Once this forms, the elongation into fibrils is rapid. Other processes of molecular assembly *in vivo* are also characterized by this nucleation-dependent pathway such as viral coat assembly, microtubule formation and flagellum formation (*19*). These processes are all characterized by a slow nucleation phase where a series of slow rearrangements occur eventually resulting in the formation of a stable nucleus of ordered monomers. This nucleus then acts as a seed allowing further assembly to proceed rapidly. Finally, the large polymers or multimeric assembly reaches equilibrium with the monomer (*19*). Because of this nucleation step, a "critical concentration" of monomer must be observed before fibrils begin to form and fibrils only grow as long as this minimum concentration of monomer is maintained. The slow nucleation phase results in a "lag time" during which the supersaturated solution remains kinetically soluble. The length of this lag phase is dependant on buffer conditions such as pH, temperature, and salt concentrations. It is also dependant upon protein concentration as well as the presence of other proteins in solution (*19*). Further proof of the nucleation-dependant model stems from seeding experiments. Here, a pre-formed fibril is added to the solution. Because the necessary nucleus is already formed, fibril assembly can continue at a rapid pace (as long as the critical concentration of monomer is maintained). Indeed, researchers have seen the disappearance of the lag phase by the addition of seed polymers in relatively small amounts (~5% by moles in some cases.) (*19*). Other theories of amyloid formation still use the nucleation model. They differ in how the monomer is converted to an amyloidogenic form, and in the nature of the rate-limiting step (*20*). In the "templated assembly" model, the amyloid polymer acts as a

template that allows for conversion of soluble monomers. In the "monomer-directed conversion" model, the soluble monomers convert to amyloidogenic forms spontaneously and thus drive nucleation by their conversion (*20*). In another model proposed, the soluble and amyloidogenic species are in equilibrium in solution. Here, the rate-limiting step is the chance convergence of those amyloidogenic species in solution and the subsequent formation of a nucleus (*20*). In any case, the nucleation model is the simplest explanation for not only the results of *in vitro* experiments, but the *in vivo* sequence of events in which symptoms of amyloid diseases take a very long time to manifest. The nucleation model is shown in the Figure 3.

The amyloidoses have garnered much attention in research recently. Over sixteen different types of amyloid proteins have been observed in amyloid deposits in clinical diseases (*21*). Amyloid fibril formation is observed in cases of Diabetes mellitus, Alzheimer's disease, Parkinson's disease, Huntington's disease, the Spongiform Encephalopathies such as Kuru, Mad Cow Disease, Scrapie, Creutzfeldt Jacob Disease and Fatal Familial Insomnia.

Alzheimer's disease is characterized by fibrillar protein deposits both intra-and extracellular to neurons in the brain. These highly-organized protein aggregates are termed amyloid plaques. These plaques consist mainly of a 39 to 43 amino acid fragment of the Amyloid Precursor Protein (APP) (*22*). This peptide (Aβ peptide) is arguably the most studied of the amyloid-forming proteins. The peptide is the result of an alternate proteolysis of APP. There at least four membrane-bound APP's produced from alternative splicing of the APP gene (*23*).

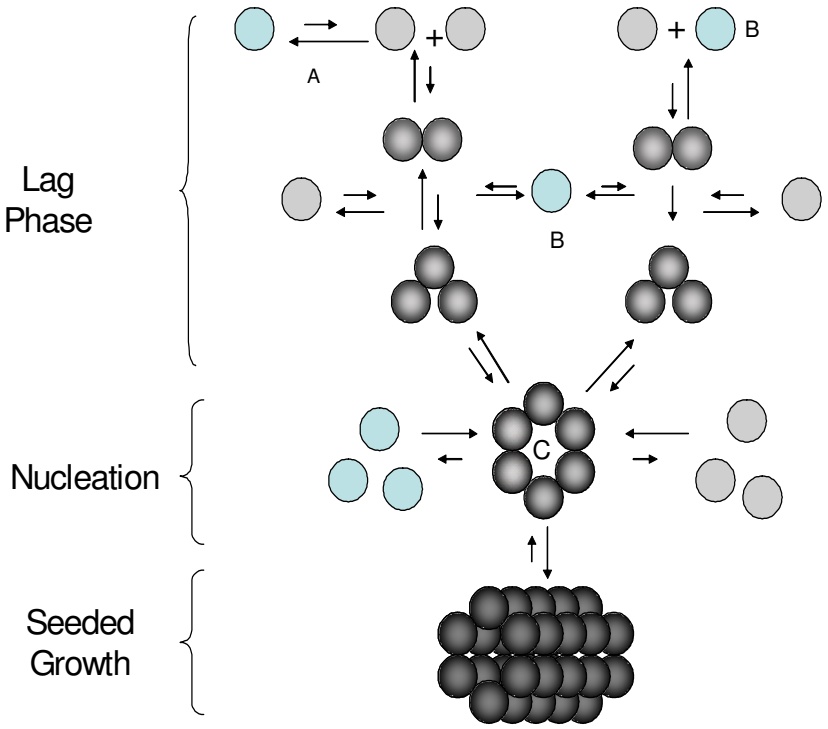

Figure 3 Proposed nucleation model of amyloid fibril formation. A) Spontaneous conversion from native to amyloidogenic form. B) Directed conversion (recruitment) of native form to amyloidogenic form by another amyloid form. C) Stable nucleus forms resulting in rapid recruitment and growth of fibril. Adapted from Harper et al. *(19).*

The APP proteins undergo a series of proteolytic cleavage events that could result in the production of the amyloid-forming peptide (*23*). If cleaved by α-secretase, APP is processed normally. However, cleavage by β- or γ-secretase results in production of the highly amyloidogenic peptide. The Aβ peptide is secreted where it interferes with cholinergic neuron function both pre-and post-synaptically (*24*). It is thought that this contributes to the eventual loss of neurons and the onset of symptoms

such as dementia and memory loss. It has been shown *in vitro* that synthetic peptides of as few as 14 amino acids from the sequence of Aβ form amyloid fibrils spontaneously (*23*).

The Spongiform Encephalopathies (Mad cow Disease, Scrapie in sheep, and it's human forms Creutzfeldt Jacob-CJD, Kuru, and Gerstmann-Sträussler-Scheinker syndrome-GSS) are other neurological diseases associated with amyloid fibril formation. Here, the prion (PrP) protein undergoes a structural change from its normal soluble form (PrP^{C}) to a structure containing much more beta sheet secondary structure (PrP^{SC}) that is proteolytically stable and accumulates in the brain. There are point mutations associated with this PrP^{SC}; however, these mutations are not always seen (*19*). This proteolytically stable structure continues to aggregate and form plaques eventually leading to cell death. Neurons are destroyed at a rapid rate. Upon necropsy, the brains have a sponge-like appearance where huge areas of neurons have been destroyed leaving holes. PrP^{SC} has been shown in the laboratory to recruit wild type soluble PrP to form more copies of this alternate structure thus propagating the disease (*19*).

Because amyloid formation is thought to be a type of aggregation, researchers have explored the possibility that sHSP's can inhibit this aggregation as they inhibit aggregation of other proteins in solution. In fact, it has been reported that there is an increase in the level of sHSP's and α-crystallins in the brains of patients diagnosed with Alzheimer's (*25, 26*). However, experimental efforts to prove inhibition of amyloidogenesis by α-crystallins have produced mixed results. Some have reported that certain sHSP's can inhibit amyloidogenesis in vitro (*22, 27*), while others have reported

that α-crystallins enhance amyloid formation and toxicity (*28*). Specifically, Kudva et al. tested the ability of several sHSP's from human and mouse to inhibit amyloidogenesis of $A\beta_{1-42}$ (*22*). They reported significant reduction in fibril formation as measured by thioflavin T fluorescence when substoichiometric amounts of both human sHSP27 and murine sHSP25 were added to the solution (*22*). This is in stark contrast to Horwitz's observation that equimolar amounts of the sHSP are necessary to inhibit aggregation of alcohol dehydrogenase or citrate synthase (*11*). Also, Kudva reported that a mixture of αA-and αB-crystallin had no ability to inhibit amyloidogenesis under the conditions used (*22*). In fact, Stege et al. reported that αB-crystallin actually enhances the toxicity of the $A\beta_{(1-40)}$ peptide (*28*). No protection against aggregation of the amyloid-forming peptide was observed. They reported that near-equimolar amounts of the crystallin increased neuronal cell death in culture. The apparent light scattering due to aggregation also increased as did thioflavin T fluorescence (*28*).

A Novel Small Heat Shock Protein from *Babesia bovis*

A protein (HSP20) isolated by our lab from the bovine erythrocyte parasite *Babesia bovis* has shown very similar activities to that of the α-crystallin sHSP's in initial *in vitro* studies. *Babesia*, a hemoprotozoan parasite, causes damage to livestock and other animals including humans (*29, 30*). These parasites are single celled organisms, which can infect erythrocytes, as well as other blood cells such as lymphocytes and histiocytes (*30*). *Babesia* species are the causative agents of "Texas red-water Fever" in cattle. The parasite is often acquired from a bite by a tick

(*Boophilus*) vector. The parasite enters the host erythrocyte and begins replication termed "binary schizogony" which eventually leads to death of the host cell (*30*). The merozoites released infect other cells and the process continues. The mortality rate in adult cattle is 90% if untreated. Symptoms include high fever, listlessness, and loss of appetite. The kidneys often excrete excess hemoglobin as a result of massive erythrocyte lysis (*30*).

Though infection of cattle is usually controlled by elimination of the tick vector, the search for effective vaccines continues. Brown et al. (*31*) have examined the possibility of developing an effective subunit vaccine based on immunostimulatory proteins produced by *B. bovis* and *bigemina*. HSP20 was not only found to be a T-lymphocyte stimulatory antigen, but also has homology to the α-crystallin family (*31*). This protein was isolated by members of our lab and is the subject of research in this dissertation.

HSP20 has limited homology to members of the α-crystallin family, with the majority of the identical/conserved amino acids occurring in the region corresponding to the α-crystallin domain. It is known that this protein can exist as an oligomer (Ficht-unpublished), but the form and structure of the protein under various solution conditions is not known. Also, the interactions between HSP20 and other proteins in solution have not been characterized. Finally, the motifs responsible for the multimerization of the protein are not known.

A recent collaboration with Dr. Theresa Good of the University of Maryland, Baltimore County has produced interesting results. It was shown experimentally that a

solution of HSP20 and $A\beta_{(1-40)}$ (BAP) formed fewer amyloid fibers than BAP alone. In a second experiment, the viability of neuronal cells exposed to a solution of BAP and HSP20 *in vitro* is greater than that of the same cell line exposed to BAP (*27*). Therefore, HSP-20 has some very interesting qualities. Characterization of this protein will yield a better understanding of the activity of this class of molecular chaperones. Also, study of this protein could lead to a more complete understanding of amyloid formation and perhaps a therapeutic strategy for the amyloidoses.

HSP20 is an intriguing protein with a great potential as a therapeutic against the amyloid diseases. A basic study of the protein and its activities was undertaken to gain a better general understanding of the protein and evaluate this potential therapeutic value. Thus, this dissertation has three specific aims. The first is a basic study of the protein HSP20 and its physical characteristics. The second aim of this dissertation is to evaluate the activity of the protein as it relates to inhibition of unwanted aggregation of proteins and specifically amyloid fibril formation. Finally, an examination of the domains controlling multimerization of HSP20 and what role they play in the activities of the protein is performed.

HSP20 was shown to have homology to α-crystallins. A more detailed analysis of the sequence and secondary structure of the protein revealed many similarities with known α-crystallins. Sequence alignments with known members of this protein family were performed to determine residues and sequences that might be important to the α-crystallin activity of the protein.

Because it has been reported on numerous occasions that α-crystallins have an inhibitory effect on the thermally-induced aggregation of certain proteins, a study of the aggregation inhibition activity of HSP20 was undertaken. Experiments were performed to confirm the activity of HSP20 with regards to inhibition of thermally-induced aggregation. The next chapter discusses a protocol similar to that developed by Horwitz displaying the inhibition of aggregation of thermally denatured proteins by α-crystallin (*11*).

Some work has been done by others indicating regions important for some α-crystallins in forming oligomers (*5, 32, 33*). These proteins were analyzed and the most likely corresponding regions in HSP20 were identified. Deletions of these possible multimeric domains were made in an attempt to affect the multimeric state of the protein. These various truncated forms of the protein were evaluated for aggregation inhibition.

The ability of α-crystallins to inhibit amyloid fibril formation and toxicity is still a point of much debate (*22, 28, 34-36*). In the following chapters, the amyloid inhibition activity of HSP20 was evaluated not only for the full-length form of HSP20, but for the truncation mutants that were found to be deficient in their ability to form multimers. Beyond gaining a better understanding of the α-crystallins and amyloidogenesis in general, it is hoped that this protein can be used to create a more effective therapeutic agent against the neurodegenerative diseases.

CHAPTER II

MATERIALS AND METHODS

HSP20 Gene Isolation

The gene encoding the HSP20 protein was isolated using a cDNA library of the genome of *Babesia bovis* created by Dr. Barbara J. Ruef. The gene was ligated into the pMAL (NEB) expression vector by Dr. Ruef then transformed into TOP10 chemically competent *E. coli* cells. A plasmid prep of this pMAL vector containing the DNA sequence for HSP20 was used as the PCR template of HSP20 described below.

Construction of Expression vector Coding for HSP20

HSP20 was produced as an N-terminal polyhistidine fusion protein (HisHSP20) in *E. coli*. A plasmid prep of the pMAL vector containing the coding sequence for HSP20 was used as a template for a PCR to amplify the HSP20 gene for ligation into the pTrcHisTOPO vector (Invitrogen). A typical PCR is illustrated below in Table 1. Primers (Table 2) were designed using MacVector (Accelrys) software and were ordered from IDT (standard desalting purification). The forward primers were designed with an intervening Tobacco Etch Virus (TEV) protease site (*37*) between HSP20 and the polyhistidine tract. This site could later be used to cleave the upstream purification tag incorporated into the recombinant protein by the expression vector. The PCR product was ligated into the pTrcHis TOPO protein expression vector (Invitrogen) and transformed into chemically competent TOP10 *E. coli* cells (Invitrogen) as directed by the manufacturer. Briefly, 4 µl of the 25 µl PCR reaction was mixed with one micro liter of vector solution. This mixture was allowed to incubate at room temperature for 5

minutes allowing the ligation of the insert into the vector to occur. Two micro liters of this solution was then mixed with one tube (~100 µl) of chemically competent TOP10 *E. coli* cells on ice. After a thirty minute incubation, the cells were heat shocked at 42°C for 30 seconds and immediately returned to ice. This suspension of cells was then added to 250 µl of SOC media and incubated at 37°C for 20 minutes shaking on an orbital shaker. Fifty to 100 µl of this culture was plated on LB agar containing 50 µg/ml carbenicillin. Truncated forms of the protein were developed using a plasmid prep from the HisHSP20 clone as a template. Primers were designed using the MacVector software as before and are listed below in Table 2. PCR products were ligated into pTrcHisTOPO vector as described above and transformed into chemically competent TOP10 *E. coli* cells.

Table 1: Typical PCR setup for HSP20 coding regions

Step	*Temperature (Time)*	*Description*
1 Cycle	95°C (15 min)	Initial melt and activation of AmpliTaq gold
30 Cycles	95°C (30 sec) 55°C (45 sec) 72°C (60 sec)	Duplex melt Anneal Elongation
1 Cycle	72°C (10 min)	Final Elongation

Recombinant HSP20 Preparation

Transformed cells were plated on LB agar with 50 µg/ml carbenicillin. Colonies were picked and streaked on new plates of LB agar and 50µg/ml carbenicillin. Those streaks were picked and suspended in PCR mix. A "colony screen" PCR was performed using a set of primers that contained one primer that annealed to vector and one primer that annealed to the insert. This PCR mix results in a reaction that only produces the correct sized product if the insert is in the proper orientation within the vector. Streaks corresponding to clones with the correctly sized and oriented insert were confirmed b sequence analysis and stored permanently as freezer stocks in 50% glycerol at -80°C.

Table 2: Primers used in generating coding regions of HSP20

Primer Name	*Sequence*	*Annealing Temperature (°C)*	*Features*
Full-Length HSP20 Forward Lab # F32901	5'-GAA AAT CTT TAT TTT CAA GGT ATG TCG TGT ATT ATG AGG TGC-3'	68.2	Contains TEV protease site coding region
Full-Length HSP20 Reverse Lab # F32901	5'-CTA TTA GGC CTT GGC GTC AAT CTG AAC-3'	67.0	Contains stop codon
C-del HSP20 Reverse Lab # H40501	5'-CTA TTA AGA GAA TTG AGA GCA CTC GAT CC-3'	64.2	Contains stop codon
N-del HSP20 Forward Lab # D52101	5'-GAA AAT CTT TAT TTT CAA GGT ATT CCT CCT CCT AAG GAG TTG GAG AAC-3'	71.1	Contains TEV protease site coding region

HSP20 Protein Purification

HisHSP20 was prepared by growing cells in LB broth at 37°C containing 50μg/ml carbenicillin to OD_{600} of 0.5 followed by induction with 1mM IPTG for 5 hours, and removal of media. Cultures of cells induced with IPTG were collected by centrifugation at 8000xg for 20 minutes and 4°C. The supernatant was removed and the cells were suspended in lysis buffer (6M Guanidinium-HCl, 0.5 M NaCl, 20 mM phosphate buffered at a pH of 7.8) followed by probe sonication (usually ten 30 second bursts using a Dynatech 150 Dismembrator). Nickel resin (ProBond Resin from Invitrogen) was prepared according to manufacturer recommendations for a denaturing purification of the target protein.

The cell lysate was clarified by centrifugation at 5000xg for 10 minutes and was incubated with the prepared nickel affinity resin for 1-2 hours to allow binding of HisHSP20. The resin was then separated from the lysate by gravity or low speed centrifugation and washed several times each with two to three column volumes of two denaturing wash buffers at pH's 7.8 and 6.0 respectively (Invitrogen ProBond Resin kit). The resin was finally washed in pH 6.0 wash buffer with 50mM imidazole to remove any trace contaminants still associated with the resin. The proteins were eluted from the resin using 50 mM EDTA in a one step batch elution, followed by dialysis overnight into PBS pH 7.0, 20% glycerol and frozen at –20^{o}C. Protein purity and molecular weight were confirmed by SDS PAGE. A protein prep for all four forms of the protein is shown in Figure 4.

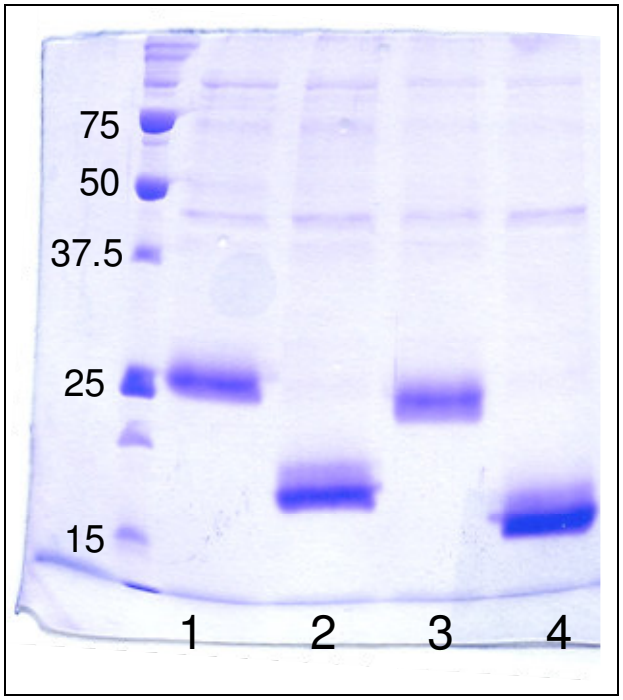

Figure 4 SDS PAGE (12% polyacrylamide) of purified HisHSP20 forms. BioRad Broad Range markers in left-most lane with molecular weights in kDa listed. Samples of full-length HisHSP20 (lane 1), N-terminal deletion NHisHSP20 (lane 2), C-terminal deletion CHisHSP20 (lane 3) and NC double deletion mutant NCHisHSP20 (lane 4) after nickel resin purification as described in Chapter II Materials and methods

The final recombinant protein produced contained additional amino acids due to the expression vector purification tag and TEV protease site. The primary amino acid sequence of the full-length HisHSP20 protein is shown in Figure 5. The coding sequence of HSP20 begins at amino acid 43 (Figure 5) of the recombinant HisHSP20. The truncation mutants have these same 42 amino acids preceding their coding sequences as well.

Structural Analysis of HSP20 and Deletion Mutants

Circular Dichroism Spectroscopy

CD experiments were carried out on an AVIV model 62 or 202 circular dichroism spectrophotometer. Thermal stability scans were performed using 29µM protein samples. The samples were placed in a 1mm cuvette and scanned from 250 to 200 nm in 0.5 nm increments with a 5 second averaging time at each wavelength while

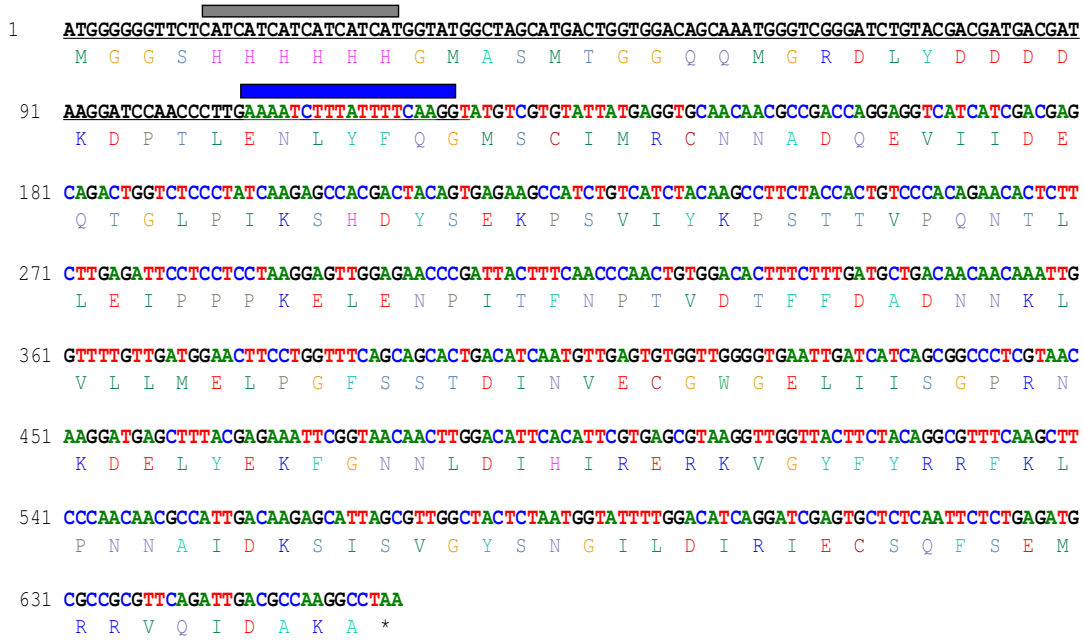

Figure 5 Primary sequence and amino acid translation of HisHSP20. Illustrated using BioEdit software. Black nucleotide sequence is from pTrcHisTOPO expression vector. His purification tag(gray bar). TEV Protease site encoded by primer (blue bar). HSP20 amino acid sequence begins at residue 43.

being stirred by a magnetic stir bar. The samples were equilibrated for 300 seconds at each temperature of 5,25,37,42 and 95 degrees before the spectrum was measured. Data was imported into Microsoft Excel spreadsheets for visualization and analysis.

Size Exclusion Chromatography

The sizes of HisHSP20 oligomers as functions of concentration and solution conditions at room temperature were determined using size exclusion chromatography on a Pharmacia FPLC system. Protein samples of 100 µl at various concentrations were loaded onto a Superose 6 HR 10/300 column (Pharmacia) and eluted using PBS (10 mM phosphate, 120 mM NaCl, pH 7.4). Eluted proteins were detected using UV absorbance at either 280 nm or 254 nm. Oligomer sizes were estimated based on the elution volumes of a set of calibration proteins run on the same column under similar conditions. The standard curve generated with the set of known molecular weight standards is shown in the Figure 6. The void volume was measured using Blue Dextran 2000 and found to be 7.81 ml. The bed volume of the column was determined by $\pi r^2 h$ to be 24.186 ml. These values were used in calculating the K_{av} for a particular elution volume using the following formula (equation 1).

$$K_{av} = (V_e - V_o)/ (V_t - V_o) \qquad (1)$$

In equation 1, V_e is elution volume, V_t is bed volume and V_o is the void volume. The value of K_{av} was determined based on each elution volume observed and the standard curve in Figure 6 was used to determine an apparent molecular weight.

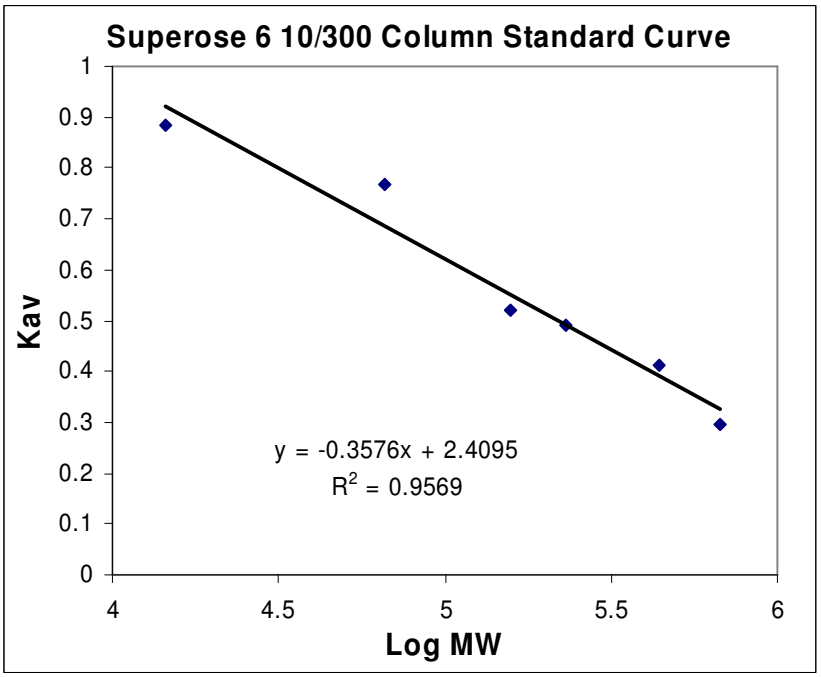

Figure 6 Plot of K_{av} vs. log of molecular weight of standard proteins eluted from Superose 6 10/300 column (Pharmacia). Elution volumes for each standard were measured and a value of K_{av} for each standard was determined using equation 1. The plot above was generated in Microsoft Excel. The equation for the line of best fit applied to the data points above was used as a standard curve in determining the apparent molecular weight of experimental samples from their calculated K_{av}.

A second column (Superdex 200 HR-Pharmacia) was used in later analyses of the truncated forms of the protein. The resolving range of this column is approximately 10 kDa to 600 kDa. The void volume for this column as determined by Blue Dextran elution was 9.795 ml and a bed volume of 23.94 ml. As before, a set of standards were eluted from this column under experimental conditions. The elution volumes were used in calculation of the K_{av} for each standard using equation 1. These values were plotted versus the log of the standards' molecular weights and a standard curve was generated (Figure 7). This column was used to separate the proteins under native conditions using PBS and 100 µl samples as above. In addition, this column was used to separate cross-linked forms of the protein under denaturing conditions. In this case, 6M guanidine hydrochloride, 500 mM NaCl, 20 mM phosphate pH 7.8 was used as the mobile phase.

Radiolabelling of Proteins

E. coli cells containing the HSP20 expression vector were grown to an OD_{600} of 0.5 in LB broth at 37°C while shaking. The cells were then pelleted by centrifugation at 8000xg and 4°C for 20 minutes followed by removal of the growth media. The cell pellets were washed with 1X M9 minimal salts media (Difco). The cells were pelleted by centrifugation again and the media was removed. The cells were suspended in minimal growth media supplemented with thiamine (0.002% w/v), glucose (0.01% w/v) and all amino acids (0.01% w/v) except methionine. Radiolabeled ^{35}S-Methionine (Amerscham Pharmacia) was added (2.5 mCi) to the media. The cells were then induced with 1mM IPTG for up to 5 hours at 37°C with shaking as described before.

Cells were harvested by centrifugation, followed by lysis and protein purification as described above.

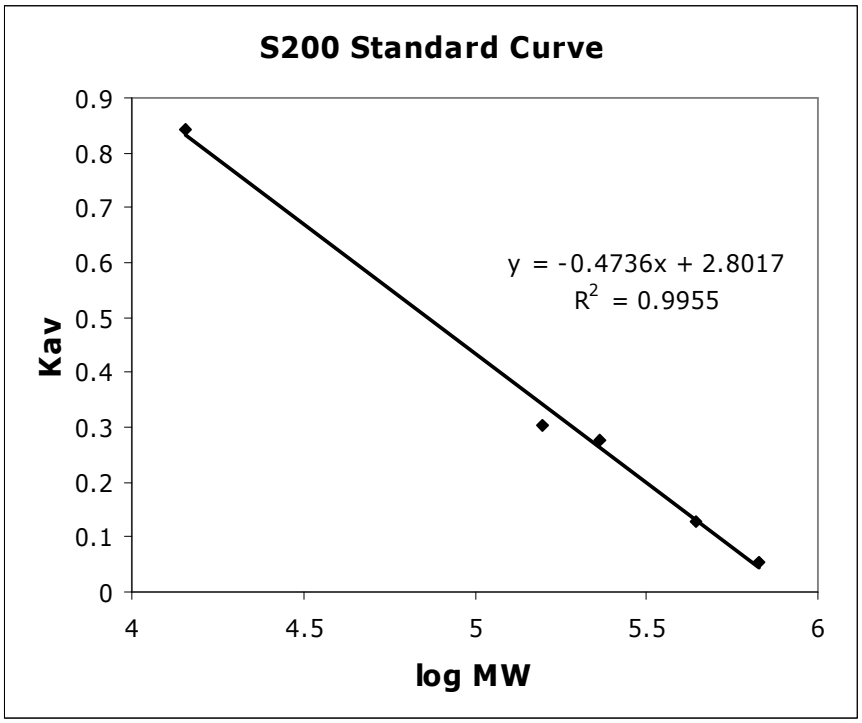

Figure 7 Plot of K_{av} vs. log of molecular weight of standard proteins eluted from S200 column. Elution volumes for each standard were measured and a value of K_{av} for each standard was determined using equation 2. The plot above was generated in Microsoft Excel. The equation for the line of best fit applied to the data points above was used as a standard curve in determining the apparent molecular weight of experimental samples from their calculated K_{av}**.**

Sedimentation Velocity Ultra Centrifugation with Radiolabeled Proteins

Purified, radiolabeled protein samples were diluted to equal concentrations in PBS. Typically, 100 µl were placed on a 5 to 30% glycerol gradient. The gradient was centrifuged in a Beckman LS-80M ultra centrifuge, SW-41 rotor at 35000 rpm

(150,000xg) for 48 hours at 4°C. The sample tubes were punctured and drained from the bottom into fractions. Typically, 12-ml volumes of gradients were created and these were fractionated into 0.5-ml fractions. Fractions were diluted to 5 mls using Ecoscint XR scintillation fluid and analyzed on a Beckman scintillation counter. The ^{35}S window was read for each sample for 2 minutes. Average values were recorded and plotted in Excel software. Plots were generated as percentage of total counts observed for each fraction versus the fraction number.

Cross-linking of Multimeric Forms Using Glutaraldehyde

The multimeric state of HSP20 forms were analyzed using a chemical cross-linker followed by separation via poly acrylamide gel electrophoresis or size exclusion chromatography. Protein samples were diluted in HGNED (1mM DTT, 100 mM NaCl, 0.2M EDTA, 0.05% v/v NP-40, 10% v/v glycerol, 25 mM HEPES, pH 8.0) buffer to the desired concentration. The samples are allowed to equilibrate before adding glutaraldehyde to a final concentration of 0.01% v/v. The reaction is quenched by the addition of a 1M Tris 1M Glycine solution at time points between 5 and 20 minutes.

PAGE Analysis

Native and Denaturing (SDS) PAGE analysis were performed on samples using the BioRad Mini Protean II system. Samples were combined with equal volumes of 2X SDS loading dye containing SDS, beta mercaptoethanol and glycerol. Samples were boiled for 5 minutes prior to running. Various gels were used including hand-poured 12% native and SDS gels as well as 4-20% gradient gels purchased from LifeGels. Gels

were stained in standard Coomassie staining solution for approximately one hour and destained over night.

Staining of Gels with SYPRO Ruby Stain

As an alternative to standard Coomassie staining of protein gels, SYPRO Ruby stain (Molecular Probes-Invitrogen detection technologies, cat # S12001) was employed using the "rapid protocol" included with the purchase of the staining solution. After the gel was subjected to electrophoresis, it was placed in 100 ml of fixing solution (50% methanol, 7% acetic acid (v/v)) for 15 minutes at room temperature on an orbital shaker. This procedure was repeated after the fixing solution was removed and replaced with fresh solution. The gel was stained with 60 ml of SYPRO Ruby gel stain by heating in a microwave at maximum power for 30 seconds followed by agitation for 30 seconds. The solution was heated an additional 30 seconds to a temperature of approximately 80°C and agitated at room temperature for 5 minutes. The sample was heated for 30 seconds in a microwave again and allowed to incubate at room temperature on an orbital shaker for an additional 23 minutes. The gel was washed in 100 ml of wash solution (10% methanol, 7% acetic acid (v/v)) for 30 minutes. Finally, the gel was washed several times with distilled water before imaging with a digital camera on a transilumination base emitting at 280 nm.

Western Blotting

Western blotting was used to confirm the presence of HSP20 forms on PAGE gels. After running gels as described above, the gel was placed in ice-cold transfer buffer (3g tris-HCL, 14.6g glycine and 20% (v/v) methanol in double-distilled H2O).and

inserted into the transfer apparatus (BioRad MINI-Protean II Transfer System) according to manufacturer's recommendations. Samples were transferred to nitrocellulose membrane (PROTRAN transfer and immobilization membrane-Schleicher &Schuell) at 100V for 1 hour in a cold circulating bath. Membranes were blocked for 1hr. in 20 ml of 3% gelatin TBS(10 mM tris, 500mM NaCl, pH 8.0) or for 3 hours in 10%(v/v) milk in TBS+0.05% Tween-20(TBST) shaking on an orbital shaker at room temperature. The membrane was washed three times with 10 ml of TBST for 10 minutes each time. Primary antiserum (polyclonal antiserum "32.12 from rabbit Sinclair 1:20"-raised in rabbits against HSP20 by Barbara Ruef 1999) was diluted 1:50 (total dilution 1:1000) in 1% gelatin-TBS (or 10% milk TBST). The membrane was incubated with 5 ml of primary antibody solution for 2 hours shaking. To visualize trace amounts of proteins in multimeric forms, the membrane was incubated with the primary antiserum in 10% milk and TBST over night at 4°C rotating on a rolling drum. The membrane was washed two times with 10 ml of TBST for 10 minutes followed by two 10 minute washes in 10 ml of TBS. The secondary antibody (goat anti-rabbit IgG H&L phosphate labeled (cat #075-1506 KPL)) was diluted 1:5000 into 10 ml of 1% gelatin TBS or 5%v/v milk in TBS. The membrane was reacted with this solution for 1 hour, shaking. The membrane was washed twice for 5 minutes in 10 ml of TBST followed by two 5-minute washes in 10 ml of TBS. The development solution consisted of one tablet of BCIP/N (Sigma) in 10 ml of double distilled H_2O. The solution was reacted with membrane until bands were easily discernable. Washing the membrane in 100mM EDTA in water quenched the reaction.

Analysis of Activities of HSP20 and Deletion Mutants

Aβ Peptide Preparation.

Aβ $_{(1-40)}$ was purchased from BioSource International (cat# 03-138) as a lyophilized trifluoroacetic acid salt. Stock solutions of 10 mg/ml Aβ(1-40) peptides were made up in 0.1% (v/v) trifluoroacetic acid (TFA) in water. The peptide stock solutions were immediately diluted to concentrations of 0.5 mg/ml by addition of sterile phosphate buffered saline (PBS; 0.01 M phosphate, 0.12 M NaCl, pH 7.4). The peptides were diluted to final concentration of 50 μM by addition of PBS for Congo red and thioflavin T analysis. These peptide solutions were combined with various amounts of different HisHSP20 forms and rotated on an orbital platform shaker in 1.5-ml Eppendorf tubes horizontally at 25°C for 24-48 hours to ensure aggregation.

Congo red Binding

Congo red studies were performed to assess the presence of amyloid fibrils in Aβ solutions. Congo red dye (Sigma) was dissolved in PBS (10 mM phosphate, 120 mM NaCl) to a final concentration of 120 mM. Congo red solution was added to the peptide solutions at the ratio of 1:9. The peptide solution and control solution were allowed to interact with Congo red for 30-40 minutes in a dark enclosure prior to absorbance measurement with a Response II UV-Vis spectrophotometer (Gilford) at 25°C. The fibril formation of the samples was estimated from the absorbance using equation 2 (*38*).

$$[A\beta_{Fib}] = ({}^{541}A_t / 4780) - ({}^{403}A_t / 6830) - ({}^{403}A_{CR} / 8620) \quad (2)$$

where [$A\beta_{Fib}$] is the concentration of Aβ fibril, $^{541}A_t$, $^{403}A_t$ and $^{403}A_{CR}$ are the absorbances of the sample and Congo red at the wavelength of 541nm and 403nm, respectively (*38*). From these data, relative fibril concentrations were calculated as the ratio of sample fibril concentration to pure Aβ fibril concentration.

Thiflavin-T Binding

Amyloid fibril formation was also evaluated by thioflavin-T fluorescence. 198 µl of amyloid samples in PBS were combined with 2 µl of 500µM thioflavin-T in 50mM glycine-NaOH buffer, pH 8.5. Samples were loaded on 96-wel fluorescence plates and evaluated using a Molecular Dynamix Gemini II fluorescence plate reader. Excitation wavelength of 444 nm and emission wavelength of 485 nm were used.

ADH Turbidity Assay

Light scattering of alcohol dehydrogenase (ADH) and HSP20 was performed as previously described (*11*). Briefly, the aggregation of ADH and HSP20 in solution was measured by the apparent absorption due to scattering at 360 nm in a Gilford Response II spectrophotometer. HSP20 concentrations were varied to obtain different molar ratios of Hsp20 to ADH. Initial experiments were performed as a time course at 58^{o}C using the Thermoset attachment (Gilford) with readings being taken once every minute for up to 90 minutes. Later experiments were performed after a 20 minute incubation at 58°C followed by a single absorbance reading at 360 nm.

CHAPTER III

CHARACTERIZATION OF HSP20

Introduction

The protein HSP20 isolated from the bovine erythrocyte parasite *Babesia bovis* was initially characterized as a member of the α-crystallin family of small heat shock proteins. This was determined using the BLAST database comparison software available to the public via the internet. Though bioinformatics indicated the structural motifs of the protein to be consistent with other α-crystallins, a more extensive study was performed to confirm this classification. The form of the protein purified and studied below also incorporates the 6-histidine purification tag. This form has an additional 42 amino acids on the N-terminus of the wild type protein and is designated HisHSP20.

The following results section contains analyses of the full-length form of HisHSP20. First, structural studies of the protein were performed using secondary structure prediction algorithms and circular dichroism. The stability and overall secondary structure of HisHSP20 was determined. The multimerization of HisHSP20 was explored using various techniques such as gel electrophoresis, and size exclusion chromatography. The effects of solution conditions and concentration on the multimeric population of HisHSP20 were examined. Finally, an evaluation of the chaperone activity of HisHSP20 was performed. Using protocols developed previously (*11, 27*), the thermally induced aggregation of ADH and amyloid formation of Aβ peptide were evaluated in the presence of various amounts of HisHSP20.

Results

Structural Studies of HisHSP20

Table 3 contains basic chemical information for HisHSP20 such as calculated pI and molecular weight (*39, 40*).

Table 3: Basic chemical parameters of HisHSP20

Number of Amino acids	*Molecular Weight*	*Theoritical pI*	*Extinction Coefficient*[a]
219 (174 code for HSP20)	24,897 Da	5.13	17670

[a] Extinction coefficient is in units of M^{-1} cm^{-1}, at 280 nm assuming all Cys residues appear as half cystines

The primary sequence of HSP20 is reported in the following sequence alignment (Figure 8). Also contained in this alignment are other known members of the α-crystallin family (*M jannaschii* HSP 16.5 (*15*) and wheat HSP16.9 (*6*)). The putative α-crystallin domains as well as the N and C-terminal domains are indicated in Figure 8 as as reported by Sun et al (*1*). The α-crystallin domain of HisHSP20 was identified using Motif Scan software (*41*) to be from amino acid 74 to 174. Though there is limited sequence homology between these three proteins, there is significant secondary structural homology as determined by PSIPRED software (*42, 43*). The secondary structural elements are indicated as blue bars (alpha helices) and green arrows (beta sheets).

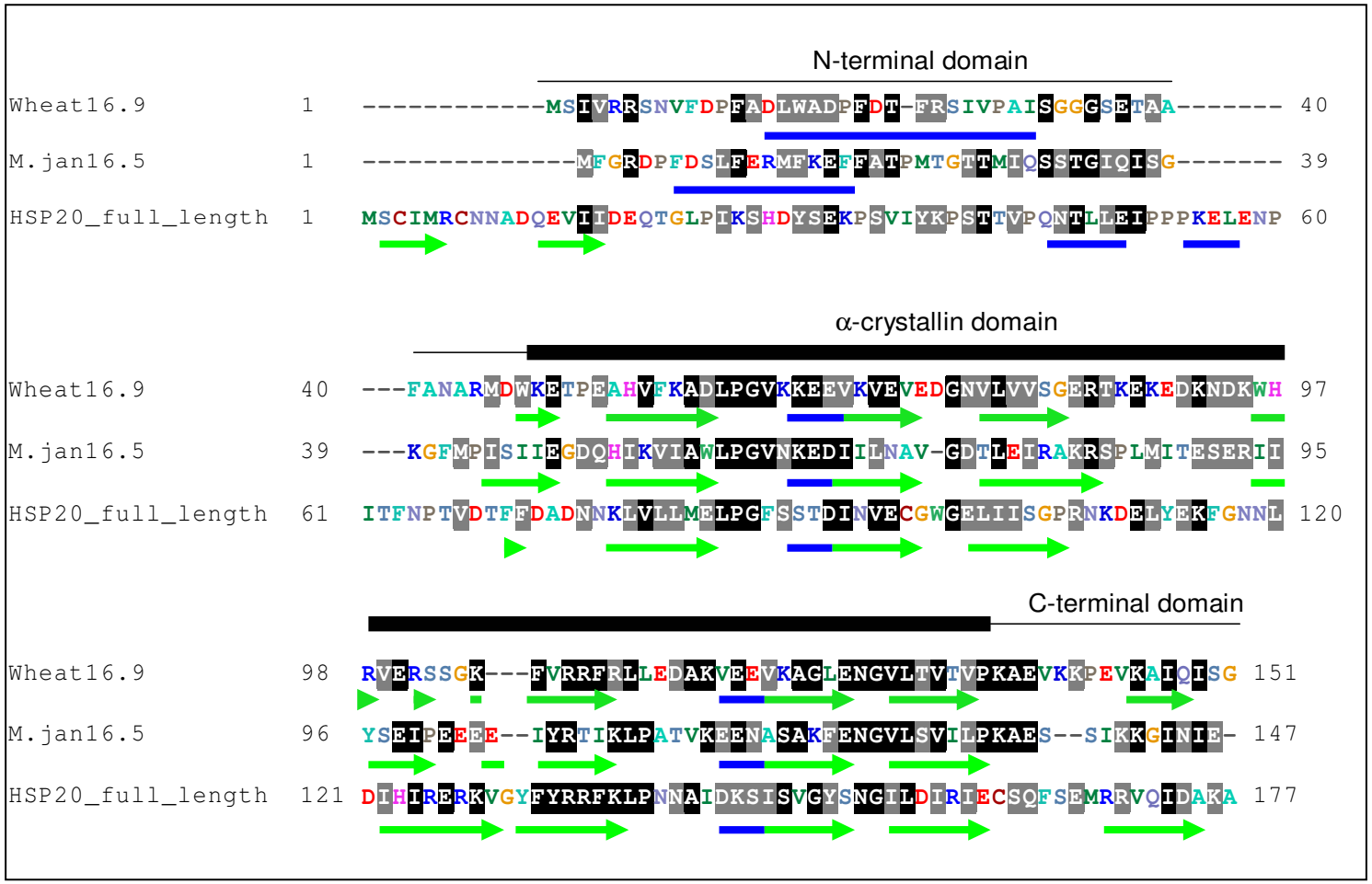

Figure 8 Sequence alignment of full length HSP20 with *M. jannaschii* 16.5 and wheat HSP16.9. ClustalW 1.82 was used for alignment. Identical amino acids are labeled black, conserved residues are labeled grey. Secondary structure elements as predicted by PSIPRED software: Alpha helices (blue bars) Beta sheets (green arrows). N and C terminal and α-crystallin domains were determined by Sun et al.(*1*)

Though the amino acid sequence homology is fairly low, the majority of the identical/conserved residues occur in the region classified as an α-crystallin domain. In fact, the amino acid homology between *M. jannaschii* 16.5 and wheat 16.9 is also low. The group of α-crystallins varies markedly in their primary amino acid sequence while the secondary structural elements are very similar. The secondary structure prediction shows a similar beta-sheet region in all the proteins corresponding to α-crystallin domain areas. There are specific amino acid residues that have previously been determined to be very important to the function of *M. jannaschii* HSP16.5 and wheat 16.9. For example, in a previous chapter, it was noted that Arg107 in *M. jannaschii* 16.5 and Arg 108 in wheat 16.9 are highly conserved (*6*). This residue is conserved in HSP20 as well at residue 134 (Figure 8). This and other regions are discussed in more detail at the conclusion of this chapter.

Secondary Structure Measurements of HisHSP20

Cicular dichroism is used to determine overall secondary structure of proteins in solution. Beams of left- and right-circularly polarized light are absorbed differently by protein molecules. Different secondary structure configurations such as beta sheet and alpha helices have distinct CD spectra (*44*). Figure 9 illustrates the different spectra observed for some common secondary forms of poly-lysine.

Alpha helical secondary structure is characterized by a spectrum with two minima at 208 and 222 nm while beta sheet structure results in a spectrum with a single minimum at 217 nm. Random coil structure has one minimum at about 195 nm (Figure 9). The spectra depicted in Figure 9 are used as standards of spectra obtained for these secondary structural elements (*44*).

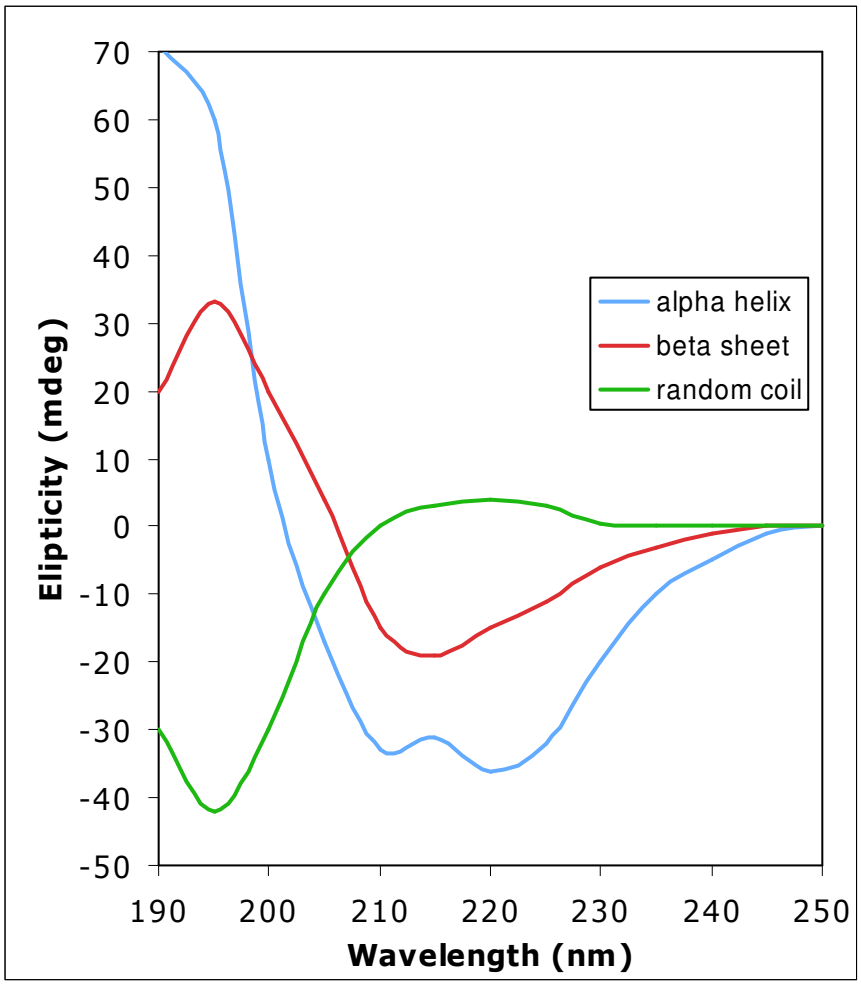

Figure 9 Model circular dichroism spectra of poly-lysine in three secondary structures. Alpha helix (blue) is shown with two minima at 208 and 222 nm. β-sheet (red) is shown with minimum at 217 nm and random coil (green) with a minimum at 195 nm *(44)*.

A number of major parameters of protein activity and stability were investigated for HSP20 to probe the variety of functions this molecule may perform. In light of the requirements for thermal insulation activities of this protein, the thermal stability of HSP20 was evaluated. Heat shock proteins are inherently stable over a broad temperature range, thus they remain active in the most adverse of conditions. To explore the thermal stability of HisHSP20, the secondary structure of the protein from 5°C to 95°C is monitored using circular dichroism. Figure 10 displays the CD spectra of the protein at several temperatures. The single minimum at ~217 nm in Figure 10 indicates a predominance of β-sheet secondary structure. Also, the intensity of the signal is relatively unchanged over the temperatures evaluated. From the standpoint of secondary structure, the protein is very stable over the temperature range of 5 to 95°C.

Studies of the Multimeric Forms of HisHSP20

The ability of the α-crystallins to form multimers in solution has been documented numerous times. The multimeric population can be over a wide range of polydisperse species or monodisperse in nature (*4, 17, 45-47*). HSP20 forms multimers in solution as well. This was first illustrated by gel electrophoresis and is shown in Figure 11. Polyclonal rabbit antiserum was raised against a truncated form of HSP20 prior to these studies. This antiserum was used to probe western blots (see Chapter II) of the protein under various conditions in an attempt to visualize the multimeric state of the protein. Using native PAGE analysis, multimeric forms of the protein were observed.

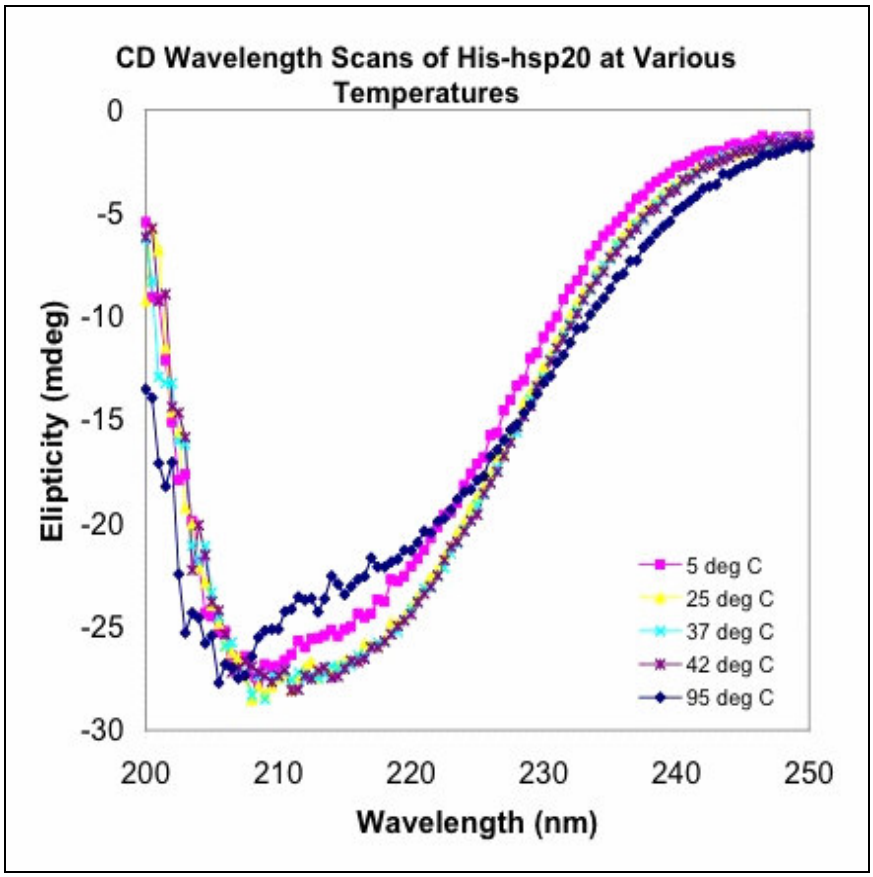

Figure 10 Far UV CD Spectra of 29 µM full-length HisHSP20 in 10 mM phosphate, 120 mM NaCl from 5 to 95°C. Samples were equilibrated at each temperature for 5 minutes prior to reading. Pathlength was 1 cm.

In Figure 11, two native gels loaded with 80μM samples of HisHSP20, one stained with Coomassie, the other analyzed by western blot are shown. The majority of the protein fails to migrate into the gel with the Coomassie staining only showing protein at the very top of the gel. But clearly, other bands are visible using the polyclonal antiserum. These bands correspond to multimeric forms of the protein. Under these conditions, the protein forms a polydisperse population of multimeric species in solution. The vast majority of the protein however is still in very large complexes which do not migrate into the gel enough for proper resolution.

Another strategy used to visualize multimers of the protein involves the use of covalent cross linking. HisHSP20 was allowed to come to equilibrium under a set of solution conditions and the chemical cross-linker glutaraldehyde was added to covalently link any multimeric species. The cross-linker was quenched at specific time points in order to 'capture' the multimers at various stages. The samples were analyzed by SDS gel or SEC. A time course of cross linking of HisHSP20 is shown in Figure 12. In Figure 12A, samples of HisHSP20 cross-linked for 0, 10 or 20 minutes were separated on a 4-20% gradient SDS gel and stained with SYPRO Ruby fluorescent stain. At time 0, the majority of the protein is a monomer as evidenced by the band migrating with the 25kDa standard in the left hand lane. In as little as ten minutes, the majority of the monomer (25 kDa) has been cross linked into some large species. The resolution of the gel is from 10 kDa to 250 kDa. Thus, in very little time, large cross-linked aggregates of the protein are seen**.**

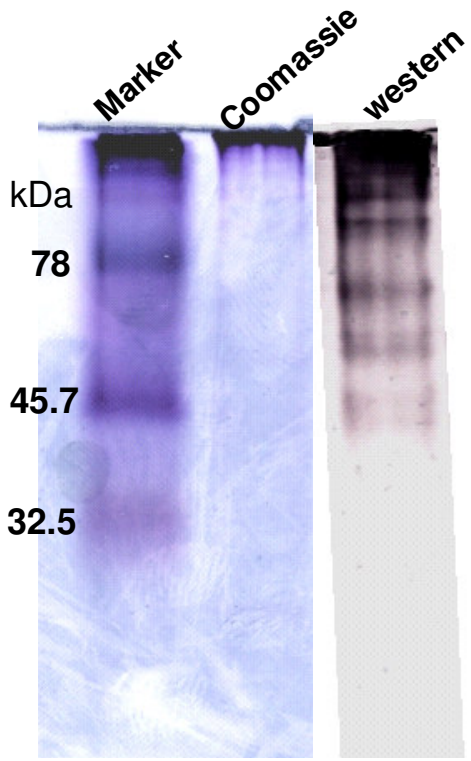

Figure 11 Native PAGE of HisHSP20 stained with Coomassie or detected via western blot. Multimers of purified HisHSP20 at 80 µM concentrations were separated on a 12% native gel and stained with Coomassie (middle lane) or were transferred to nitrocellulose membrane and probed with polyclonal antiserum raised against HSP20(right lane). BioRad Kaleidoscope marker in left lane is shown with corresponding molecular weights in kDa.

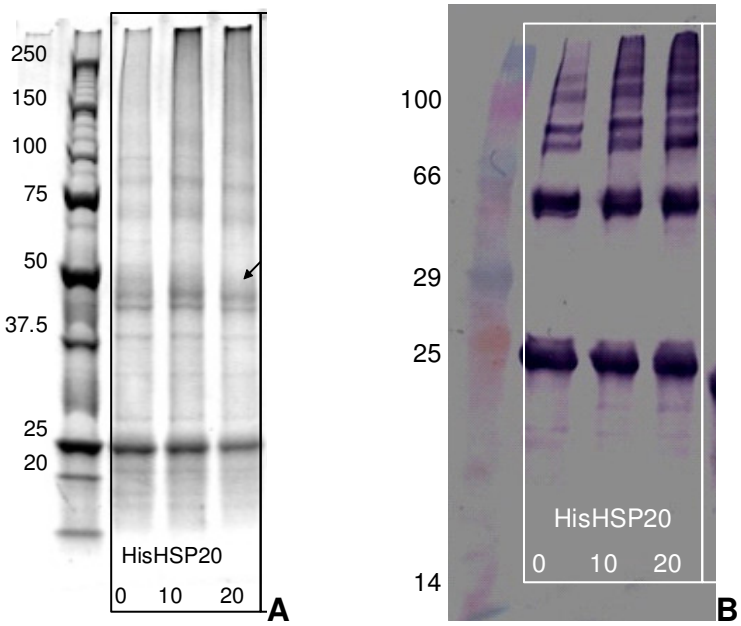

Figure 12 SDS PAGE (4-20% gradient) separations of cross-linked samples of HisHSP20. **A)** Equimolar samples were equilibrated at room temperature prior to glutaraldehyde cross-linking. Cross-linker was quenched at 0, 10 and 20 minutes and samples of each time point (indicated by labels below lanes) were separated on gel. Broad Range Precision Molecular weight Standards (BioRad) is shown in left-hand lane with molecular weights in kDa. Arrow indicates dimeric form of the protein. Stained with SYPRO Ruby stain (BioRad) and visualized by fluorescence from exposure to 280 nm light. B) Western blot of cross-linked samples of HisHSP20. Equimolar samples were equilibrated at room temperature prior to glutaraldehyde cross-linking. Cross-linker was quenched at 0,10 and 20 minutes and samples of each time point (indicated by labels below lanes)were separated on a 4-20% gradient SDS PAGE gel. Kaleidoscpoe marker (BioRad) is shown in left-hand lane with molecular weights in kDa. Samples were blotted to nitrocellulose membrane and probed using antiserum raised against HSP20 as described in Chapter II.

In Figure 12B, a western blot of HisHSP20 cross-linked under the same conditions and separted on the same type of gel is shown. Clearly, several multimeric forms of the protein are visible. It is interesting to note that the sample with no cross linker added (0 time point) still exhibits the multimeric forms of the protien to a great degree despite the presence of SDS in the running buffer. From these results, we concluded that HisHSP20 forms a polydisperse population of multimers in solution.

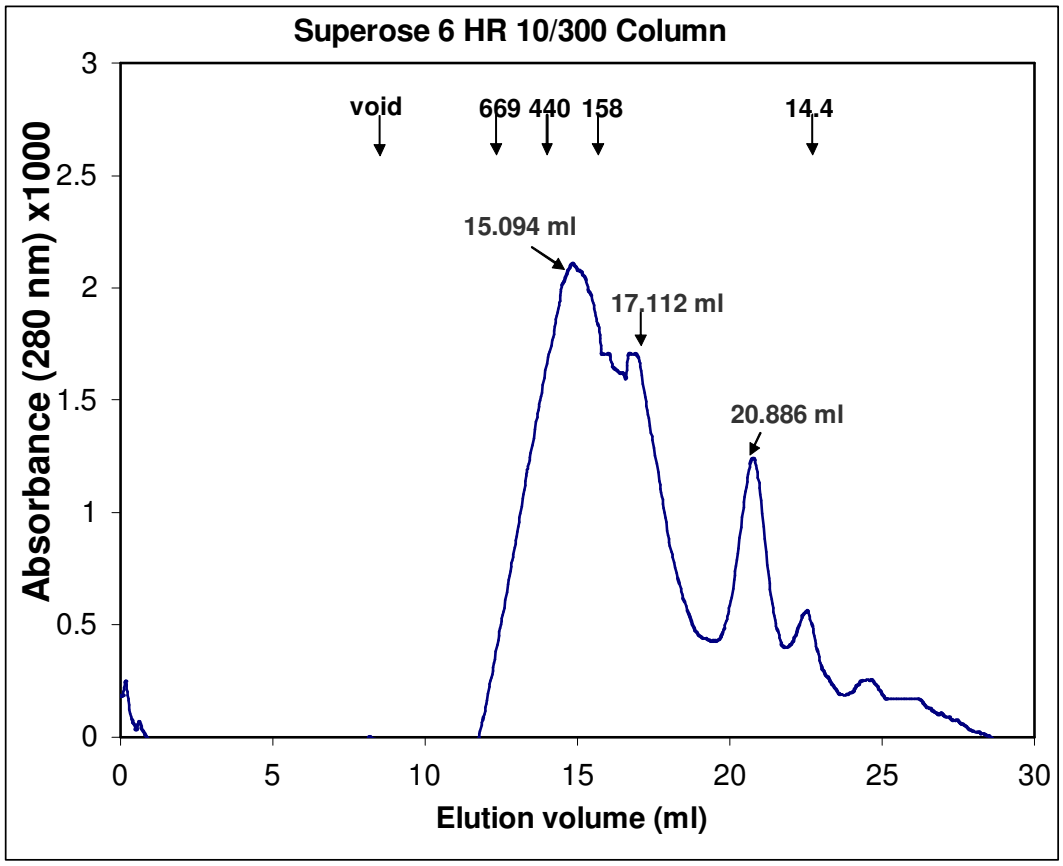

Figure 13 Elution profile of full-length 100 µM HisHSP20 from a Superose 6 10/300 column. HisHSP20 elutes over a broad range corresponding to molecular weight s from 45 kDa(dimer) to 261 kDa (decamer) relative to size exclusion standards indicated at top of graph: thyroglobulin (669 kDa), ferritin (440 kDa), aldolase (158 kDa) and lysozyme (14.4 kDa). Void volume is indicated for column at 7.81 ml. HisHSP20 at 100 µM in 10 mM phosphate, 120 mM NaCl pH 7.4.

The Effect of Concentration on the Multimeric Distribution of HisHSP20

Le Chatellier theorized that a system at equilibrium will react to a change in conditions in order to establish a new equilibrium under those conditions. Thus, if a multimeric form of HisHSP20 dominates a solution at one concentration, lowering the concentration should allow for the establishment of a new equilibrium with fewer

multimers and a subsequent increase in smaller multimer and monomer forms. We employed size exclusion chromatography (SEC), to elucidate the multimeric state of HisHSP20. By changing the solution conditions, the multimeric population was altered.

A representative chromatogram of HisHSP20 at 100 μM is illustrated in Figure 13. The very low peak height indicates that very little protein eluted from the column. The remainder of the protein was recovered by reversing the flow of the mobile phase. This indicated that the protein never entered the separation media of the column. Extremely large complexes (or aggregates) were present as the resolving range of this particular column (Superose 6 HR 10/30) is from 5 MDa to 5 kDa. Using a standard curve (see Chapter II Materials and Methods), the elution volumes were converted to apparent molecular weights. The volumes highlighted correspond to molecular weights of 261, 142 and 45 kDa. These sizes are equivalent to the molecular weight of a decamer, hexamer and dimer respectively.

The following figure is of a chromatogram generated on the same column under the same buffer conditions, but a concentration of 0.1 μM HisHSP20. In the chromatogram in Figure 14, the only peak seen is at an elution volume of 20.184 ml. This corresponds to a molecular weight of approximately 44 kDa (a dimer).

The Effect of High Salt on the Multimeric Distribution of HisHSP20

The effect of increased ionic strength on multimeric assembly was evaluated by increasing the concentration of sodium chloride (0.5 M) in the running buffer of the SEC separation. Higher salt shields electrostatic interactions to a greater degree which resulted in a change in the multimeric population by weakening the electrostatic

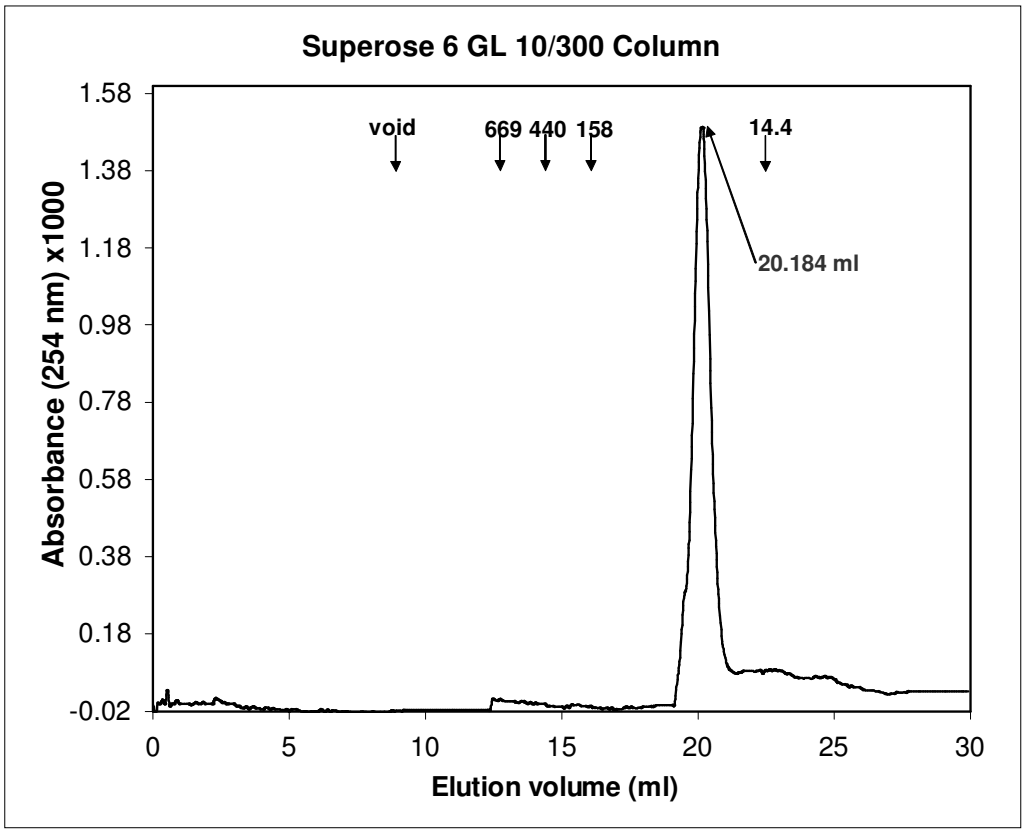

Figure 14 Elution profile of full-length 0.10 μM HisHSP20 from a Superose 6 10/300 column. HisHSP20 at 0.1 μM elutes as a single peak corresponding to molecular weight of 45 kDa (dimer) relative to size exclusion standards indicated at top of graph: thyroglobulin(669 kDa), ferritin (440 kDa), aldolase (158 kDa) and lysozyme (14.4 kDa). Void volume is indicated for column at 9.81 ml. HisHSP20 at 100 μM in 10 mM phosphate, 120 mM NaCl pH 7.4

contribution to multimerization. Figure 15 depicts an elution profile of HisHSP20 in 10mM phosphate, 50mM NaCl. The dimeric form predominates (peak D in Figure 15) with other multimeric forms ranging from hexadecyl to monomeric eluting as well. The area under the curve of this elution spectrum indicated that over 90% of the protein did

not elute from the column. This dynamic polydisperse population of multimers is influenced significantly by solution conditions.

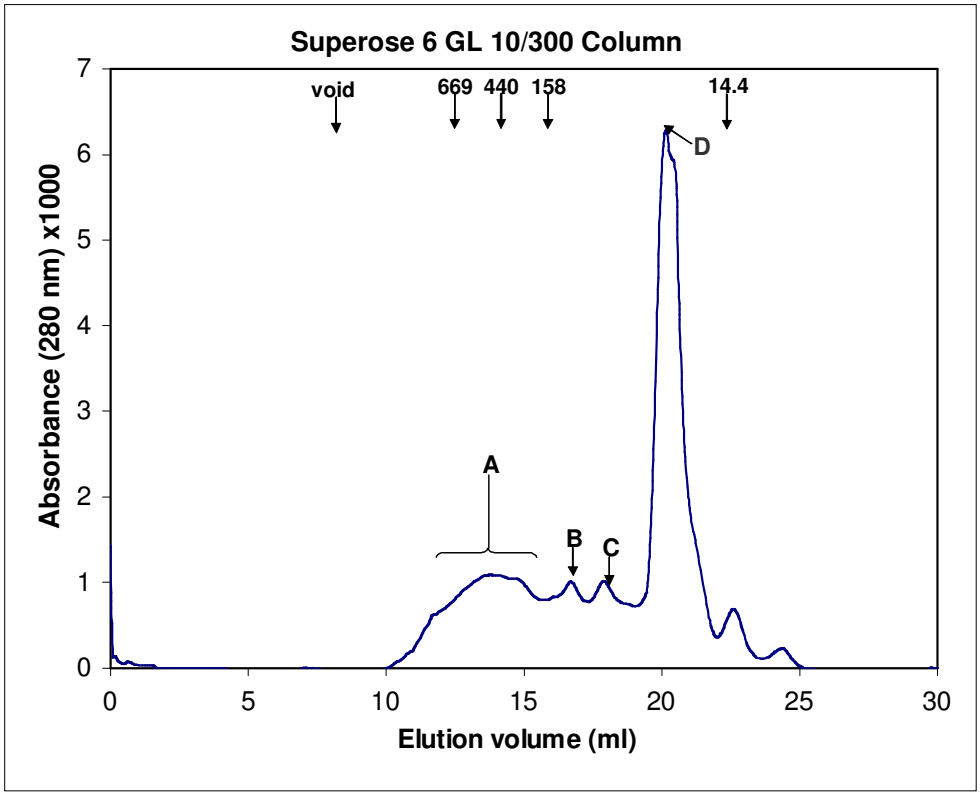

Figure 15 Elution profile of full-length HisHSP20 from a Superose 6 10/300 column in the presence of 500 mM NaCl. HisHSP20 at 29 µM elutes as a series of peaks corresponding to molecular weights A)399-264 kDa(hexadecamer to decamer), B)153 kDa (hexamer), C)109 kDa (tetramer) and D)56 kDa (dimer) relative to size exclusion standards indicated at top of graph: thyroglobulin (669 kDa), ferritin (440 kDa), aldolase (158 kDa) and lysozyme (14.4 kDa). Void volume is indicated for column at 9.81 ml. HisHSP20 at 100 µM in 10 mM phosphate, 500 mM NaCl pH 7.4

Another separation technique employed was sedimentation velocity via analytical ultracentrifugation. Glycerol gradientts (5-30%) were used to provide resistance to samples of radiolabeled HisHSP20 as they were centrifuged at 150,000xg for 48 hours at 4°C as described in Chapter II. The various multimeric forms migrate along the gradient at different rates determined by their size and shape. The result from one such experiment is shown in Figure 16.

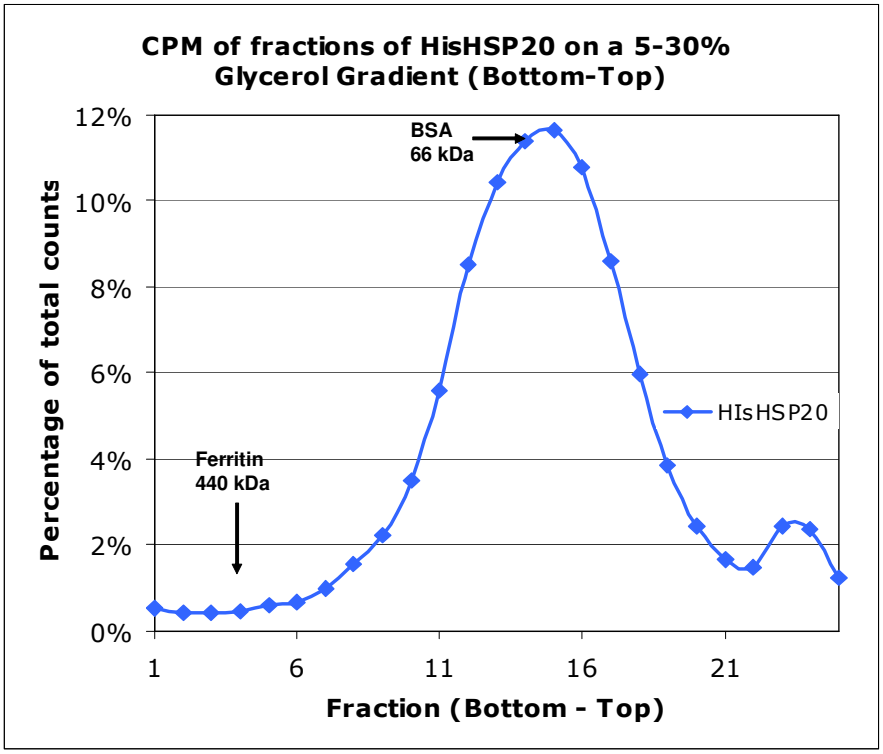

Figure 16 Elution profile of ^{35}S radiolabeled full-length HisHSP20 from a 5-30% glycerol gradient. Sample was centrifuged at 150,000 xg for 48 hrs. at 4°C. Fractions were collected from bottom of gradient and radioactivity was read using scintillation counting. Percentage of total counts for each sample is plotted vs. fraction number. Molecular weight standards of ferritin (fraction 4-440 kDa) and bovine serum albumin (fraction 14-66 kDa) were detected by absorbance of each fraction at 280 nm in a separate gradient ran under the same conditions.

In this figure, a broad symetrical peak centered around fraction 15 of the 12-ml gradient is detected as well as a minor peak at fraction 23 near the top of the gradient. The major peak indicates several multimeric species in the population. Two standards (ferritin MW 440 kDa , 17.6 S and Bovine Serum Albumin, 66 kDa and 4.3 S) are shown eluting at fractions 4 and 14 respectively for reference. The leading edge of the large peak at fraction 11 corresponds to 8.3 S and a molecular weight of 178 kDa (7.4 times the molecular weight of monomeric HisHSP20). The broad peak elutes over 13 fractions indicating a broad dispersion of multimers.

The hypothesis that a broad population range of multimeric species were present in solution under the condtions tested, is supproted by all these experiments. (SEC, PAGE and sedimention velocity). Dilution of the protein results in an equilibrium shift to a population of smaller oligomeric species which can also be observed under high salt conditions again indicating that the protein forms extremely large and dynamic complexes whose distribution is affected greatly by solution conditions.

Activities of HisHSP20

As stated in Chapter I, one of the activities commonly observed of an α-crystallin is the inhibition of thermally-induced aggregation. Thus, one of the first experiments performed on HSP20 was based on Horwitz's protocol (*11*) in which the aggretaion of alcohol dehydrogenas (ADH) at high temperature is arrested by the presence of a bovine α-crystallin. Similar protocols have been used to evaluate α-crystallins using ADH and other proteins such as citrate synthase as substrates for thermal denaturation/aggregation (*48-63*). As an evaluation of chaperone activity, the aggregation of ADH in the presence

of HisHSP20 at elevated temperature was monitored as described in Chapter II using apparent light scattering of the sample at 360 nm.

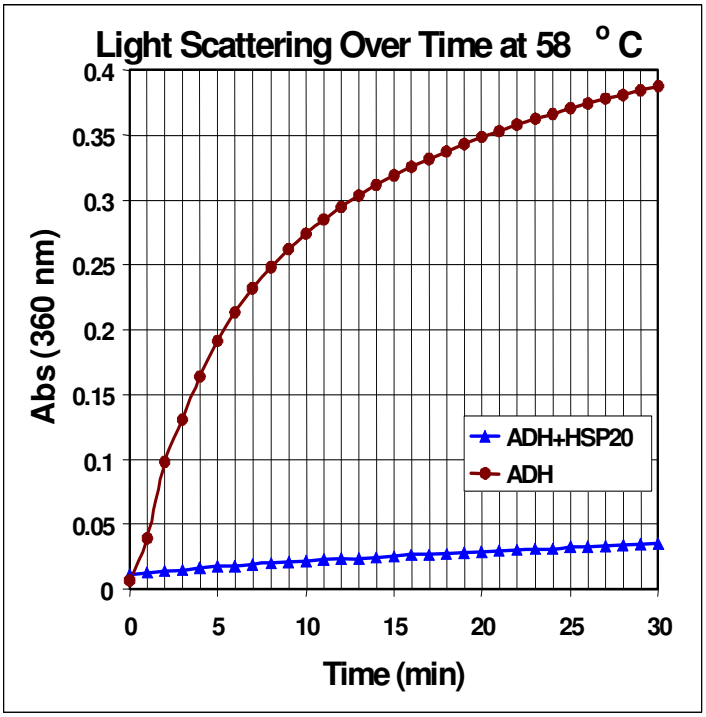

Figure 17 Aggregation of ADH in presence and absence of HisHSP20 at elevated temperature. Measurements of apparent light scattering (turbidity) of solutions at 58°C vs. time. ADH alone (red circles) exhibits a dramatic increase in absorbance at 360 nm due to aggregation within 20 minutes. ADH+HisHSP20 (blue triangles) shows significantly less turbidity. ADH at 3.25 µM, HisHSP20 at 5µM.

A representative result of this apparent light scattering of ADH in the presence and absence of HSP20 is illustrated in Figure 17. The absorbance at 360 nm of a solution of ADH at 58°C (red circles of Figure 17) increased dramatically over time. When HisHSP20 is combined with ADH in solution (blue triangles of Figure 17), a

dramatic reduction in absorbance at 360 nm was observed indicating less aggregation of the substrate ADH. In this experiment, a molar ratio of HSP20 to ADH of 1.54:1 was used.

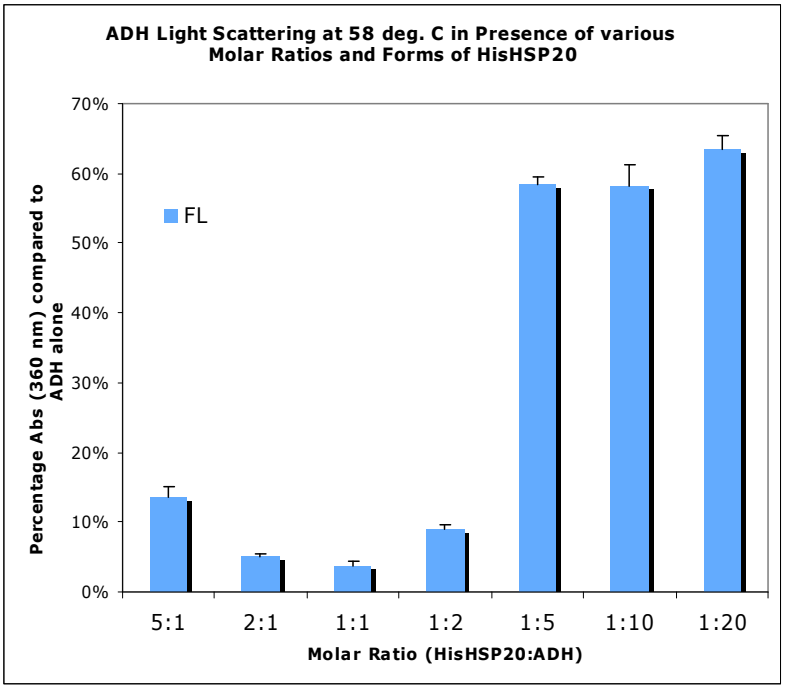

Figure 18 Apparent light scattering of ADH in the presence of different amounts of HisHSP20. The concentration of ADH is kept at 3.25 E-6 M. Molar ratios of HisHSP20 to ADH are indicated on x-axis. Samples were incubated for 20 minutes at 58°C prior to measuring absorbance at 360 nm. Absorbance of each sample was compared to absorbance of a sample of ADH alone. The percentage of absorbance compared to that of the ADH standard is plotted on the y-axis for each molar ratio. Error bars are 1 SEM. n=3

In order to evaluate the effect of concentration of HisHSP20 on its inhibition of

thermally induced aggregation, a series of molar concentrations of HSP20 were combined with ADH and the same light scattering assay was performed. Figure 18 illustrates the thermal insulation activity of HSP20 for ADH over varying molar ratios. In this experiment, one absorbance reading at 360 nm was taken of each solution after exposure to elevated temperature for 20 minutes.

The ratios of 2:1, and 1:1 (HisHSP20: ADH) show the largest reduction in light scattering at greater than 90% each (Figure 18). As the molar ratio is decreased, the protection against light scattering (apparent aggregation) is reduced. At a 1:5 molar ratio, little protection is seen. This is comparable to Horwitz's work with bovine αA-crystallin (*11*). It was also noted in Figure 18 that as the concentration of HisHSP20 was increased, the apparent light scattering increases (molar ratio of 5:1 in Figure 18). This increase in concentration is accompanied by a change in the multimeric distribution of HisHSP20 according to the earlier SEC results. This is indicative of an equilibrium shift toward a less active form of HisHSP20. In any case, it is clear that HisHSP20 is an inhibitor of aggregation under these experimental conditions.

As discussed earlier, there have been conflicting results concerning the activity of α-crystallins and inhibition of amyloid fibril formation. A series of experiments are described below detailing the activity of HisHSP20 with respect to amyloidogenesis. Full-length HisHSP20 was placed in solution with amyloidogenic $A\beta_{(1-40)}$ peptide (BAP) and allowed to incubate at room temperature in an effort to observe any inhibition of fibril formation by BAP. The samples were analyzed after 24 hours of incubation using Congo red dye binding and thioflavin T fluorescence. A representative result of

HisHSP20 in solution with BAP at several molar ratios is shown in Figure 19. Interestingly, amyloid inhibition is seen at certain molar ratios and not at others. This data correlates with data collected by Dr. Theresa Good's lab (formerly of TAMU Chemical Engineering Dept. and currently at University of Baltimore at Maryland Department of Chemical Engineering) which showed an even lower range of effective molar ratios (1:1000 to 1:1 million of HisHSP20 to BAP) (*27*).

It is very interesting to note that at a molar ratio of 1:1, the protein seems least effective at inhibiting amyloid formation and even seems to promote formation. This is a quite different result from the thermally-induced aggregation of ADH shown earlier where equimolar amounts of HisHSP20 are needed to inhibit aggregation of ADH. However, the same trend of a specific substoichiometric range of concentrations resulting in inhibition of amyloidogenesis is observed in both cases.

Summary and Discussion

Here it has been established that the novel protein HSP20 exhibits activities typical of those observed in α-crystallins. The protein has significant structural homology to other known members of the small Heat Shock Proteins (*M jannaschii* 16.5 and wheat 16.9). The protein is stable over a wide temperature range and it seems to form very large and dynamic ordered complexes as other α-crystallins have been shown to do. The protein has been shown to inhibit the thermally induced aggregation of alcohol dehydrogenase as well. This is a common trait shared with many (if not all) α-

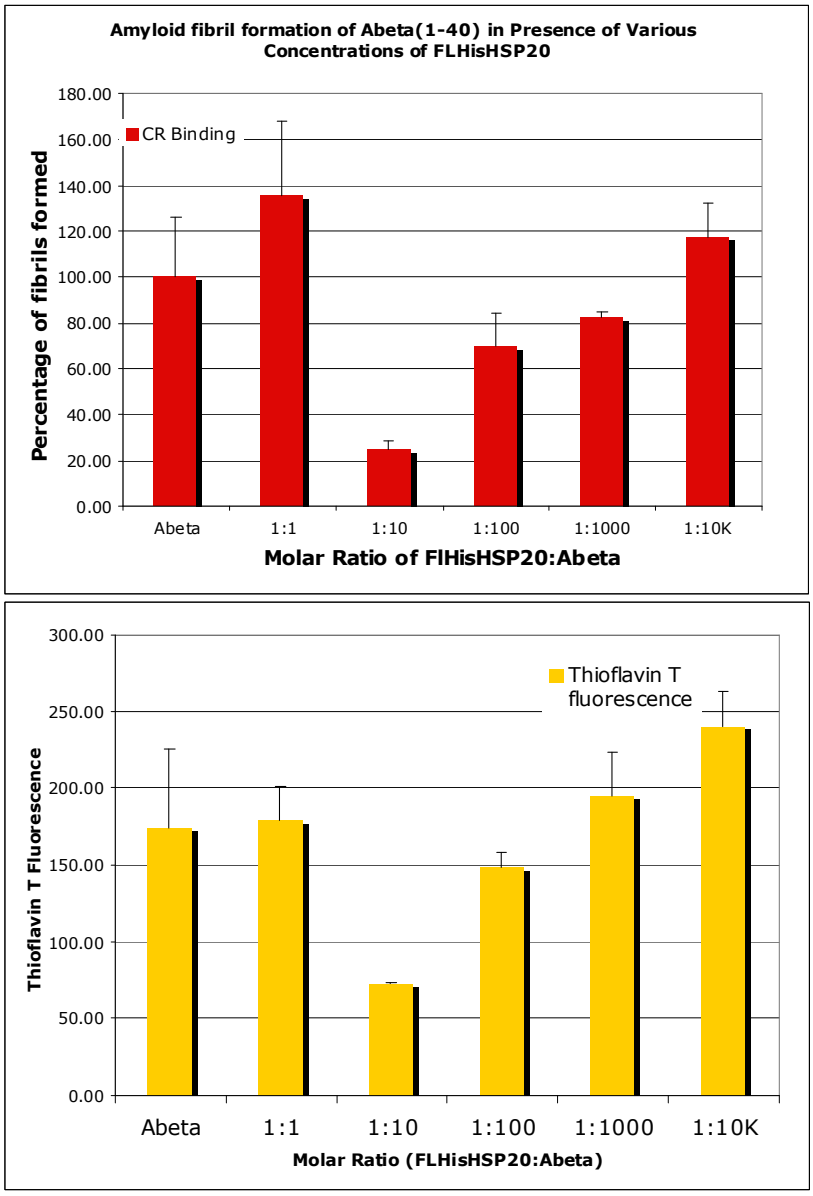

Figure 19 Inhibition of amyloid fibril formation by full-length HisHSP20. Samples of $A\beta_{(1-40)}$ were incubated at room temperature for 24 hours alone or in the presence of different amounts of HisHSP20. Concentration of $A\beta_{(1-40)}$ is kept at 50 μM. Molar ratios of HisHSP20 to $A\beta_{(1-40)}$ are indicated on x axes. Samples were analyzed by Congo red binding (top) or thioflavin-T fluorescence (bottom) as described in Chapter II. Congo red binding in top panel was used to calculate amount of fibrils formed using equation 1. Amount of fibrils formed in each sample was compared to amount of fibrils in a sample of $A\beta_{(1-40)}$ alone. The percentage of fibrils compared to that of the $A\beta_{(1-40)}$ standard is plotted on the y-axis for each molar ratio. Error bars are 1 SEM. n=3 for each molar ratio.

crystallins. Finally, the protein can inhibit amyloid fibril formation of BAP under the conditions tested and is most effective in sub-stoichiometric amounts.

Although sequence homology is relatively low, there is very significant secondary structural similarity between HSP20 and the two α-crystallins depicted in Figure 8. The large majority of beta sheets are seen in the predicted α-crystallin region for all three proteins. The residue Arg 108 was identified as very important to the function of wheat 16.9 (*6*). In fact, it is one of the most highly conserved residues in all α-crystallins. The sequence alignment shows that this amino acid is conserved in HSP20 as well in the form of residue 134. The residue is also present in the *M. jannaschii* homolog as Arg 107. It is speculated that this residue is important in assembly modes of the multimers thus relating quaternary structure to function (*6*). It is pointed out by Sun et al. (*1*) that residues 83 to 105 of wheat 16.9 are very important in dimerization of the protein as evidenced by x-ray crystal structure. This area of HSP16.9 is aligned to regions of high secondary structure homology within *M. jannaschii* HSP16.5 and HSP20 (Figure 8). Leucine 122 of *M. tuberculosis* HSP 16.3 which is equivalent to Leu 116 in *B. japonicum* HspH, was shown to be of great importance to the function of the protein. This is in the highly conserved region of GVLTVTV seen in most α-crystallins (*64, 65*). The equivalent residue is observed in HSP20 as well at residue 157, residue 129 of *M. jannashcii* and 130 of wheat HSP 16.9. These residues were shown to be paramount to function and affected the oligomerization of HspH and *M. tuberculosis* HSP 16.3 (*64, 65*). Several conserved residues within known α-crystallin domains are observed in the proposed α-crystallin domain of HSP20.

The amino and carboxy terminal regions are quite divergent in the α-crystallins. However, there is still significant homology observed in Figure 8 in these terminal regions. The functions of these regions are explored more thoroughly in the next chapter. The N-terminus is generally an unstructured and often solvent exposed region of the protein containing many hydrophilic residues. Little secondary structure has been assigned to the N-termini of the three proteins in Figure 8. The C-terminus has a fairly well conserved V/IXI/V motif present in the last 20 amino acids of many sHSP's. This small sequence is visible in HSP20 at position 158 to 160. The motif is observed at position 143-145 in *M. jannashcii* and 147-149 in wheat hsp 16.9 (Figure 8).

As the name implies, heat shock proteins are active during times of environment stress that could include, but is not limited to a temperature change in the environment of the organism. In order to be active, the proteins must be stable over a wide temperature range. The circular dichroism spectra in Figure 10 display the stability of HisHSP20 over such a range of temperatures. Even at the extreme temperatures of 5 and 95°C, much of the native secondary structure signal remains. Thus, HSP20 appears to have the stability needed to function as a molecular chaperone during times of environmental insult to the host. In fact, the protein was shown to be upregulated during environmental changes including temperature increase and oxidative stress (Ficht unpublished).

Many of the above conserved regions and residues affect the oligomeric makeup of the sHSP's. It is shown in Figures 11 through 16 that HisHSP20 forms very large multimers. In fact, these multimers are as large and diverse in population as to make their characterization problematic. By manipulating the solution conditions, the population distribution of multimers was altered (Figures 13-15). This dynamic

multimerization is another commonality between HSP20 ant the α-crystallin sHSP family.

Though it does have structural and stability attributes similar to other α-crystallins, the question of similar activity to other members of the sHSP family remained. This question is addressed in the final set of experiments in this chapter. The activity of HisHSP20 against thermal denaturation of ADH was illustrated in Figures 17 and 18. Several molar ratios of HisHSP20 to ADH were tested. The most effective ratios were found to be equimolar in nature. The apparent light scattering (and thus the thermal aggregation of ADH) increases as the concentration of HisHSP20 decreases to a molarity less than that of ADH. This is in stark contrast to the results of amyloidogenesis inhibition by HisHSP20. In Figure 19, the full-length protein is shown to inhibit amyloid fibril formation most effectively at substoichiometric amounts. In fact, this same protein was shown by Lee et al. to inhibit amyloid fibril formation at very low substoichiometric levels of 1:1000 to 1:100,000 of HisHSP20 to ADH (*27*). In this particular set of experiments, the protein is still most effective at a molar ratio of 1:10 (HSP20: BAP) and was actually least effective at a molar ratio of 1:1.

In conclusion, it has been proven that HSP20 does share many structural commonalities with other known α-crystallin sHSP's. In addition to these physical similarities, the protein also behaves as known sHSP's under the conditions tested above. At this point, it remained to be seen if these activities and structural attributes could be modified by altering the domains thought to be responsible for multimerization. The creation and analysis of these deletion mutants and their activities is evaluated in the next chapter.

CHAPTER IV

DEVELOPMENT AND STUDY OF TRUNCATION MUTANTS OF HSP20

Introduction

Though quite divergent in sequence among the small heat shock protein family, many have shown the N and C termini to be of varying importance to proper assembly and function of many sHSP's. (*17, 33, 61, 66-75*). The N-terminus is often exposed to solvent and largely unstructured. This region of the α-crystallins often undergoes rapid hydrogen/deuterium exchange. A common technique used to examine the importance of the N-terminus for a particular sHSP is to delete portions of the region and analyze its effects on multimeric assembly and chaperone function. This has been done for many α-crystallins with a wide variety of results. An example cited is that of the rat αA-crystallin. Deletion of its N-terminus yields a protein with a greatly decreased activity that only assembles into dimers and tetramers (*76*). In contrast, Laksanalamai reported that deletion of the N-terminal region of their α-crystallin isolated from *P. fuiriosus* had no affect on multimerization or chaperone activity while a deletion of both the N and C termini drastically affected both activity and oligomerization (*5*).

In the following results, we describe the multimerization and chaperone activities of three deletion mutants of HSP20. These mutants were designed to exhibit altered multimerization profiles from that of HSP20 by deleting the N and C termini and keeping the proposed α-crystallin domain intact.

Results

Structural Studies of Truncated Forms of HSP20

A sHSP from the hyperthermophile *P furiosus*(Pfu-sHSP) has been studied and characterized by Laksanalamai (*5*). Unlike the two previously mentioned α-crystallin sHSP's from wheat and *M. jannaschii*, this protein forms a polydisperse array of multimers in solution similar to that observed with HSP20 as shown in Chapter III. By examining the known crystal structure of the *M. jannaschii* HSP 16.5, Laksanalamai and van Montfort noted that the extended carboxy terminus was responsible for contact between dimers (*5, 6*). Laksanalamai also showed that by deleting the N and C termini of their sHSP, the multimeric state of the protein could be altered (*5*).The researchers concluded, however, that the N-terminus was "dispensable" for multimeric assembly, unlike the αA-crystallin from rat discussed earlier (*76*) which displayed a tendency towards aggregation and displayed reduced chaperone activity after deletion of its N-terminus. Laksanalamai generated two mutants. The N-terminal 52 amino acids were deleted in one mutant (Pfu^{N52}) and the N-terminal 52 amino acids along with the twelve carboxy terminal amino acids were deleted in the other mutant ($Pfu^{N/C}$). These regions were determined by sequence alignments of the *P. furiosus* HSP with *M. jannaschii* HSP16.5 (*5*). Using techniques such as SEC and SDS PAGE analysis of cross-linked samples, the researchers showed that the $Pfu^{N/C}$ was only capable of forming dimers and had a markedly reduced thermal protection activity. The deletion of the 52 amino acids from the N-terminus (Pfu^{N52}) resulted in no change in activity and a more polydisperse population of multimers (*5*). However, the authors of this study did not report on the

behavior of a deletion mutant of only the C-terminal amino acids thought to be involved in inter-dimeric contacts.

Figure 20 Sequence alignment of HSP20 and *P furiosus* sHSP (Pfu) (*2*). Alignment used to determine potential regions involved in multimer formation. Alignment performed using ClustalW 1.82 plugin of BioEdit Software. Residue number and protein indicated on left; (-) no residue.

Figure 20 is a sequence alignment of HSP20 with the sHSP from *P. furiosis* identified by Laksanalamai (*5*). From this alignment it was determined that deletions of the last 11 and the first 50 amino acids from HSP20 could affect the multimeric state of the protein. Three truncations of the protein were created. Using primers designed to anneal within the coding region of the HSP20 gene, truncated forms of the coding region were amplified using PCR and ligated into an inducible expression vector as described in Chapter II. The truncated forms of HSP20 protein were expressd and purified in the same manner as full-length HisHSP20 (ChapterII). The three truncated forms are an N-

terminal deletion of 50 aa (NHisHSP20), a C-terminal deletion of 12 aa (CHisHSP20), and a deletion of both the N-terminal 50 aa and C-terminal amino acids (NCHisHSP20). These deletions were made in regions that were not part of the α-crystallin domain; however, the structure/activity of the protein could easily be altered or destroyed by such deletions. Approximately 36% of the full-length form is deleted in the N- and C-terminal deletion. Table 4 contains basic chemical information for the three deletion mutants.

Table 4: Basic chemical parameters of HisHSP20 deletion mutants

Protein	*Number of Amino acids*	*Molecular Weight*	*Theoritical pI*	*Extinction Coefficient*[a]
C-terminal deletion **CHisHSP20**	208 (11 C-terminal aa's deleted)	23,598 Da	5.01	17670
N-terminal deletion **NHisHSP20**	169 (50 N-terminal aa's deleted)	19,277 Da	5.29	14565
N- and C-terminal deletion **NCHisHSP20**	158 (11 C-terminal and 50 N-terminal aa's deleted)	17,978 Da	5.12	14565

[a] Extinction coefficient is in units of M^{-1} cm^{-1}, at 280 nm assuming all Cys residues appear as half cystines

Structural Studies of HSP20 Truncation Mutants

Because of these deletions, the secondary structure and stability could be greatly affected. Below is a figure showing the CD spectra of the three deletion forms at various temperatures (Figure 21). Noted immediately was the fact that the mutants lose very

little of their secondary structure over the temperature range of 5 to 95°C. This is what was observed for the full-length form (Figure 10). Another point of interest is the secondary structure of the mutants themselves. The spectra of CHisHSP20 are almost identical to that of the full-length version. However, the two N-terminal deletion mutants have identical spectra to each other, but are different from the spectra for the Full-length and C-terminal deleted forms. The spectra have a strong beta sheet signal that is actually more centered at the typical absorbance at 217 nm than the spectra of either the full-length form or CHisHSP20. In Figure 8, it was observed that the N-terminal fifty amino acids of HSP20 had little secondary structure. It is likely that removing this region of the protein (as was the case with the two N-terminal deletion mutants) caused a loss of the random coil CD signal from that region. This allowed the predominantly beta sheet secondary structure that remained to be clearly visualized by CD.

Studies of the Multimeric Forms of Truncated Versions of HSP20

The deletions made in HisHSP20 were designed to alter the multimeric population of the protein in solution. As with the full-length form of HisHSP20 in Chapter II, glutaraldehyde cross-linking was employed to capture multimeric forms of the deletion mutants for comparison to the multimeric forms observed for the full-length form. Samples of the protein were exposed to the cross linking agent for up to 20 minutes. After quenching the cross-linker with glycine, the samples were examined using SDS PAGE and western blotting or size exclusion chromatography under denaturing conditions.

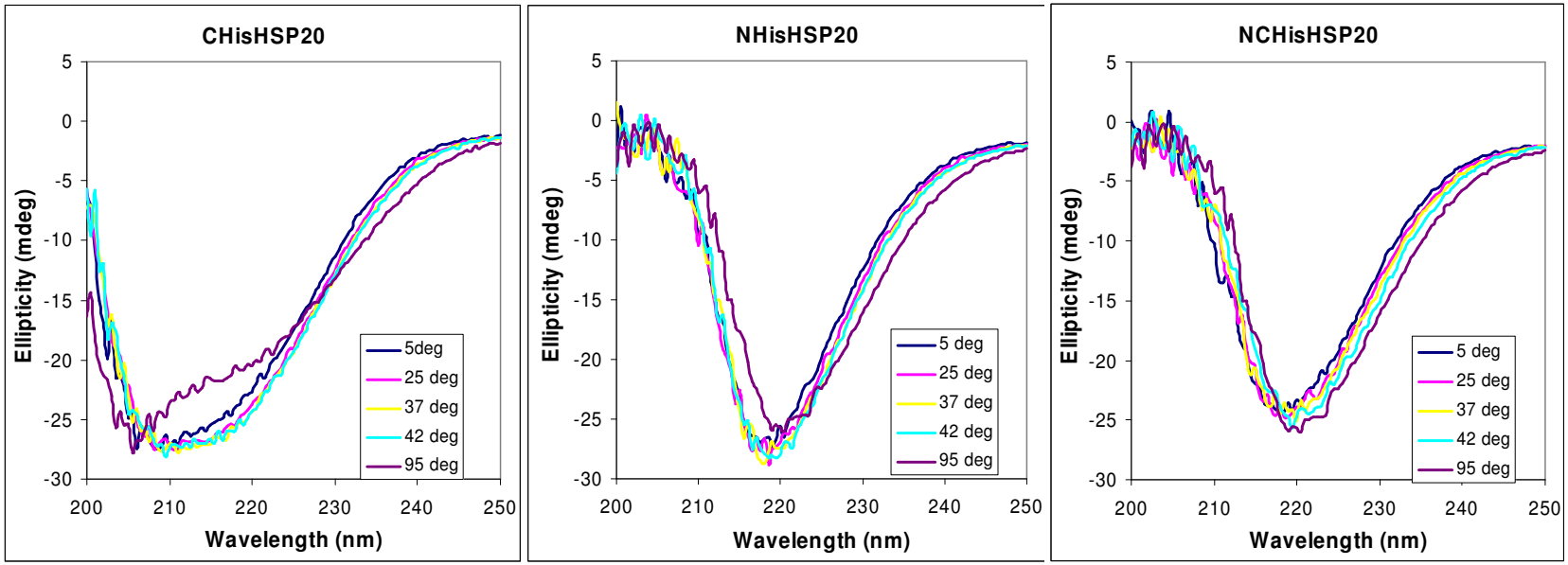

A B C

Figure 21 Far UV CD Spectra of 29 µM samples of C-terminal deletion HSP20 (CHisHSP20), N-terminal deletion HSP20 (NHisHSP20) and NC deletion HSP20 (NCHisHSP20) in 10 mM phosphate, 120 mM NaCl from 5 to 95°C. Samples were equilibrated at each temperature for 5 minutes prior to reading. Path length was 1 cm

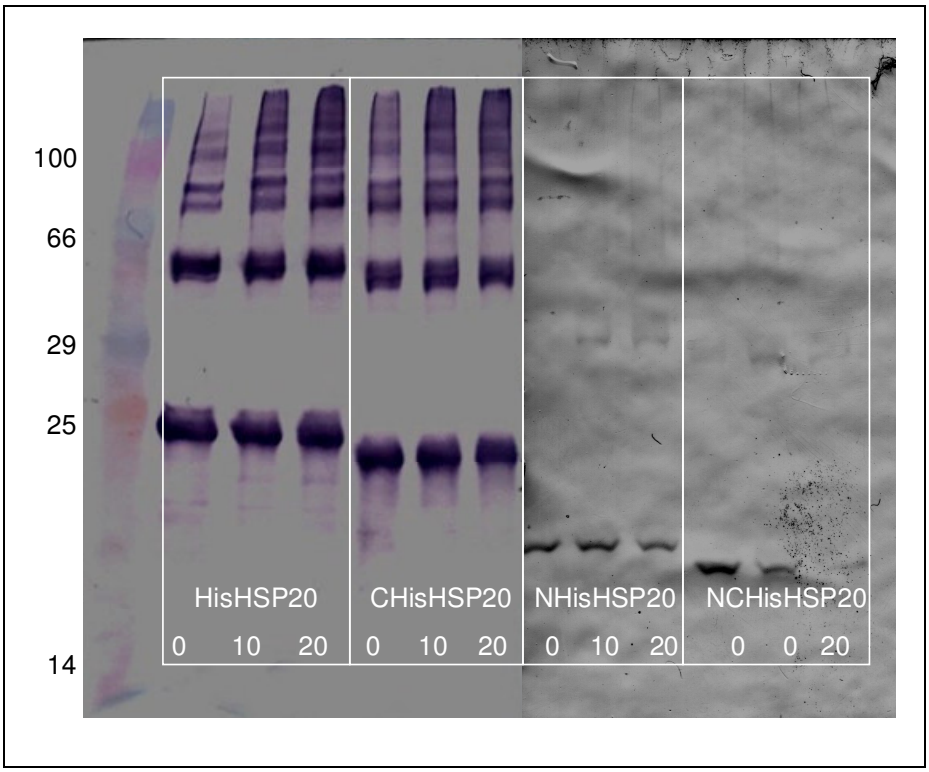

Figure 22 Western blot of cross-linked samples of HisHSP20 and its deletion mutants. Equimolar samples were equilibrated at room temperature prior to glutaraldehyde cross-linking. Cross-linker was quenched at 0,10 and 20 minutes and samples of each time point (indicated by labels below lanes)were separated on a 4-20% gradient SDS PAGE gel. Kaleidoscpoe marker (BioRad) is shown in left-hand lane with molecular weights in kDa. Samples were blotted to nitrocellulose membrane and probed using antiserum raised against HSP20 as described in Chapter II.

Figure 22 is a western blot depicting the 4 forms of the protein generated in this study after exposure to 0.01% glutaraldehyde for 10 and 20 minutes at room temperature. It was immediately evident that the C-terminal deletion of HSP20 results in a lesser degree of multimerization, but does not eliminate multimerization as evidenced by the 0 time point in Figure 22 for CHisHSP20. Deletions in the N-terminal deletions results in no multimers larger than a dimer at any appreciable levels.

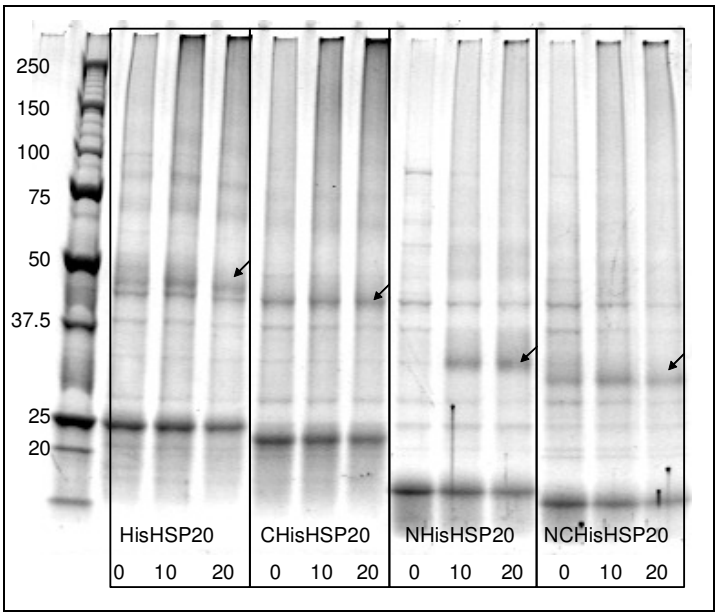

Figure 23 SDS PAGE (4-20% gradient) separations of cross-linked samples of HisHSP20 and its deletion mutants. Equimolar samples were equilibrated at room temperature prior to glutaraldehyde cross-linking. Cross-linker was quenched at 0, 10 and 20 minutes and samples of each time point (indicated by labels below lanes) were separated on a 4-20% gradient SDS PAGE gel. Broad Range Precision Molecular weight Standards (BioRad) is shown in left-hand lane with molecular weights in kDa. Arrows indicate dimeric forms of each protein. Stained with SYPRO Ruby stain (BioRad) and visualized by fluorescence from exposure to 280 nm light.

Figure 22 illustrates the fact that electrophoresis in the presence of SDS is not sufficient to destroy the natural multimeric formations of the proteins. This is especially evident in the cases of the full-length and CHisHSP20 forms. Note at the 0 time points for both, where no cross-linking agent was added, the multimers are clearly visible on the blot. Unfortunately the polyclonal antiserum used in the above western blot does not have the same affinity for the two N-terminal deletion mutants. Very little staining of these proteins is seen even after a longer incubation time with antibody. To visualize the protein throughout the gel, it was stained with SYPRO Ruby stain as shown in Figure

23. The use of this fluorescent stain allows visualization of the larger multimeric species not seen in previous Coomassie stained samples (Figure 11). It is clearly seen in Figure 23 that the full-length form of HisHSP20 and CHisHSP20 form much more of these large species (100 kDa and above) than the two N-terminal deletions. The same molar amounts of proteins were placed in each well and the cross-linking was performed on identical concentrations of proteins in identical volumes.

By using a denaturant such as guanidinium hydrochloride, all tertiary and quaternary structure was destroyed leaving only those multimers that were covalently cross-linked by glutaraldehyde. The cross-linked multimers were analyzed by separation via SEC in the presence of 6M guanidinium HCl. As can be seen in Figure 24, the truncated forms of the protein exhibit a reduced tendency to form multimers. HisHSP20 not exposed to the cross-linker eluted from the S200 column at 21.5 ml (corresponding to the monomeric form) under denaturing conditions. The next peak at 16.5 ml corresponds to an intermediate multimer. The final peak is located in the void volume of the column and corresponds to a very large (greater than 600 kDa) species. The inset allows for greater visualization of the two smaller elution peaks of interest.

In Chapter III, size exclusion chromatography was used in an effort to analyze the multimeric forms of the protein under native conditions**.** However, the majority of the protein was not seen in the eluted volume of the column unless very low concentrations of proteins were applied to the column (Figures 13-15). Because the deletions of the N and C termini of HSP20 altered the oligomeric equilibrium of the proteins from that of the full-length form, the elution profile of the truncated forms would also be different.

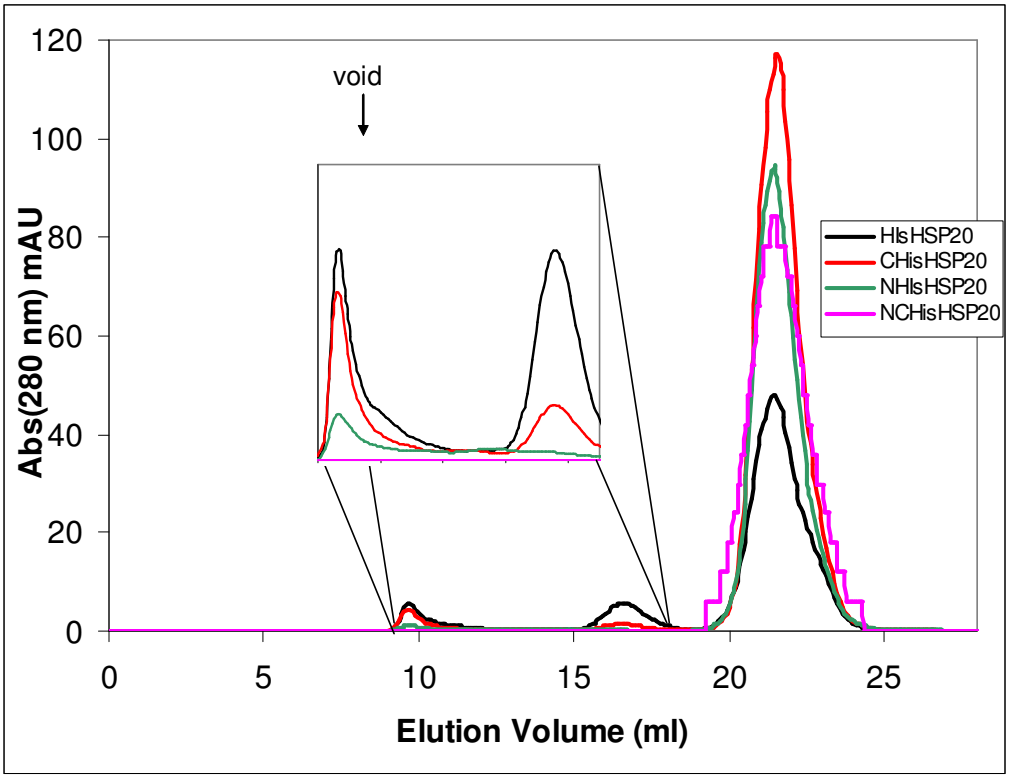

Figure 24 Elution profiles of full-length HisHSP20 and its deletion mutants from a Superdex 200 column. Samples were cross linked with glutaraldehyde for 10 minutes after equilibration at room temperature prior to separation on the column. Mobile phase contains 6M guanidinium hydrochloride, 10 mM phosphate, 120 mM NaCl pH 7.4. Void volume of 9.81 ml is indicated in figure

In Figure 25, the Superose 6 10/300 GL column used to analyze the full-length protein was employed to examine the truncated forms of the protein. A very different profile of elution was observed from that of the full-length form of the protein. A peak eluting at the apparent molecular weight of a dimer(~20.2 ml) was seen in a much greater amount for all three deletion mutants than that observed for the full-length version of HisHSP20 (Figures 13-15). By measuring the area under this curve and comparing it to the total absorbance of an equimolar sample at 280 nm, it was estimated that approximately 50 to 75% of the total protein had eluted from the column for the two C-terminal deletion

mutants. The N-terminal deletion mutant had a smaller dimeric elution peak (about 20-30% of the protein eluted). It is also interesting to note that a peak corresponding to a large molecular weight is seen in the case of the N-terminal deletion mutant.

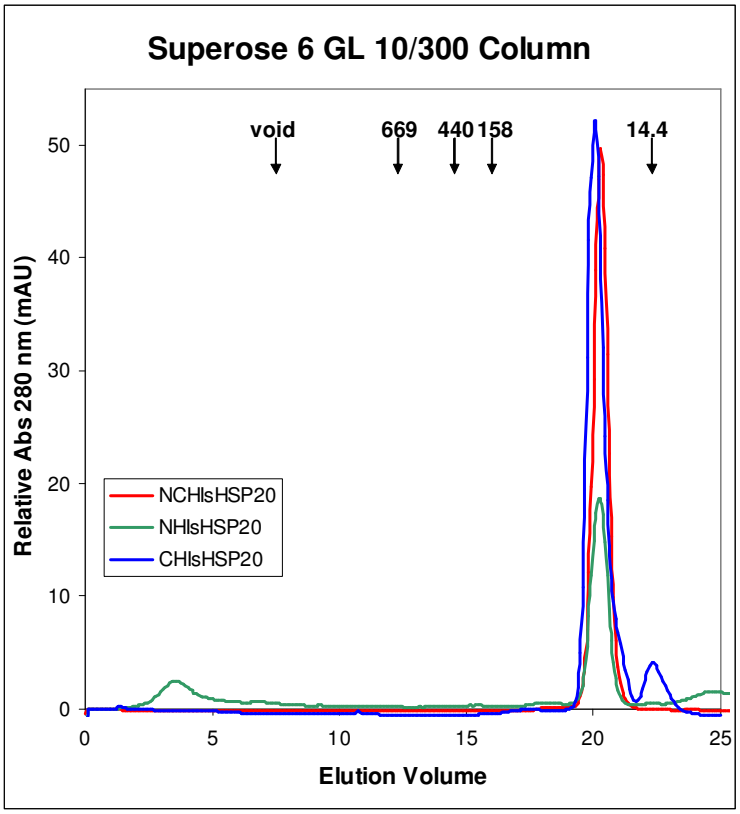

Figure 25 Elution profile of HSP20 deletion mutants from a Superose 6 10/300 column. Samples at 29 µM eluted largely as a single peak corresponding to molecular weight of a dimer for each mutant relative to size exclusion standards indicated at top of graph: thyroglobulin(669 kDa), ferritin (440 kDa), aldolase (158 kDa) and lysozyme (14.4 kDa). Void volume is indicated for the column at 7.81 ml. Mobile phase and sample buffer was 10 mM phosphate, 120 mM NaCl pH 7.4

This peak corresponds to a very large species as it eluted before the void volume of the column and was not observed every time this experiment was performed. The C-terminal deletion mutants showed no such peak.

Again, much of the protein is not seen using SEC. Therefore, the total population was visualized using a glycerol gradient as described before with the full-length form of HisHSP20 (Chapter III). The proteins were radiolabeled with ^{35}S-methionine and purified. They were placed on a 5-30% glycerol gradient and spun for 48 hours at 150,000xg (Figure 26). As in the case of the CD spectra of the various forms, CHisHSP20 displayed a very similar profile to that of the full-length form of the protein with one peak centered at fraction 12. The two N-terminal deletion mutants have very similar profiles to one another, but are very different from HisHSP20 and CHisHSP20. In this case, the gradients had two regions of protein density. The peak near the center of the gradient (fractions 10 to 17) is still present for both forms of the protein. However, these peaks were smaller and broader than those observed for the C-terminal deletion. Also, there was much more signal at the bottom of the gradient corresponding to pelleted protein and possibly insoluble HSP20.

Elution at fraction 12 resulted in a calculated sedimentation coefficient-value of 7 and an apparent molecular weight corresponding to that of a heptamer (141 kDa) of the CHisHSP20 proteins. This is very similar to the result obtained when the full-length version of the protein was exposed to this gradient in Chapter III (Figure 16). The

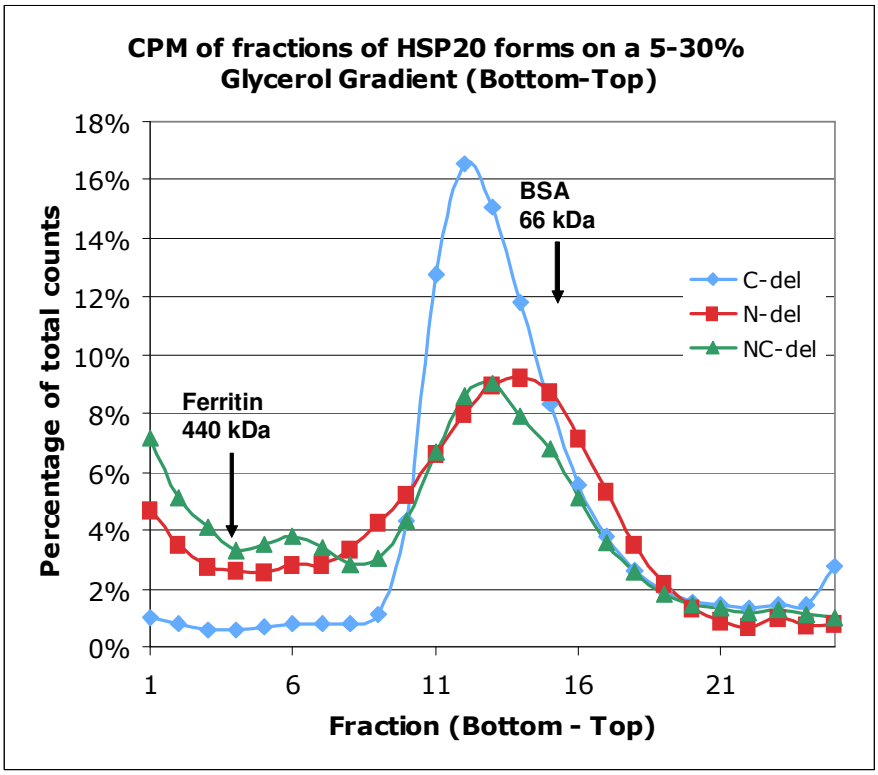

Figure 26 Elution profile of ^{35}S radiolabeled HisHSP20 deletion mutants from a 5-30% glycerol gradient. Samples were centrifuged at 150,000 xg for 48 hrs. at 4°C. Fractions were collected from bottom of gradient and radioactivity was read via scintilitation counting. Percentage of total counts for each sample is plotted vs. fraction number. Molecular weight standards of ferritin (fraction 4-440 kDa) and bovine serum albumin (fraction 14-66 kDa) were detected by absorbance of each fraction at 280 nm in a separate gradient ran under the same conditions

leading edge of the CHisHSP20 peak (fraction 10) has an apparent molecular weight of ~200 kDa (a decamer) and an S-value of 11.

Activities of Truncated Forms of HSP20

How do these deletions affect the activity of the proteins with respect to their ability to inhibit aggregation? Using the ADH light scattering technique described in Chapter II, it was shown that the proteins have the same level of specific activity as the

full-length form of the protein (Figure 27). The results of light scattering inhibition by the full-length form are included in the figure below for comparison. Equimolar ratios of HisSHP20: ADH were most effective in inhibition of the thermally-induced aggregation of ADH under the conditions tested. All proteins displayed an equal specific activity against this thermal aggregation. Thus, activity of the protein is not measurably affected by deletion of the N and C termini despite the effects on multimerization observed for the deletion mutants.

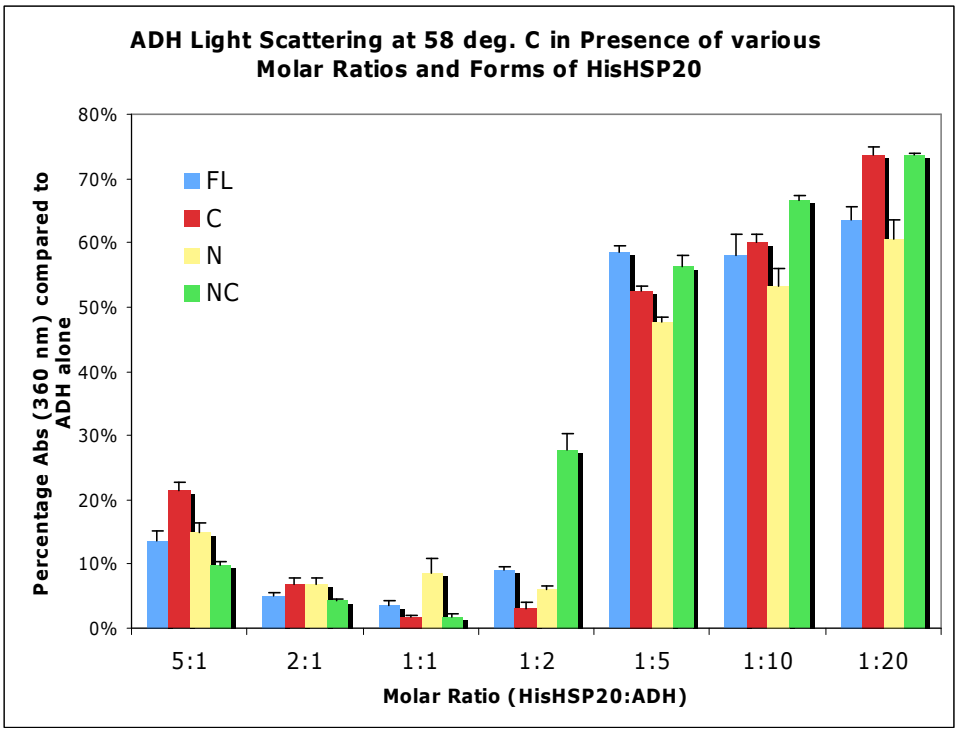

Figure 27 Apparent light scattering of ADH in the presence of different amounts of HisHSP20 forms. The concentration of ADH is kept at 3.25 E-6 M. Molar ratios of HisHSP20 form to ADH are indicated on x-axis. Samples were incubated for 20 minutes at 58°C prior to measuring absorbance at 360 nm. Absorbance of each sample was compared to absorbance of a sample of ADH alone. The percentage of absorbance compared to that of the ADH standard is plotted on the y-axis for each molar ratio. Error bars are 1 SEM. n=3

Though the inhibition of thermally-induced aggregation is unchanged after deleting the N- and C-termini, the inhibition of amyloid fibril formation by $A\beta_{(1-40)}$ (BAP) must be evaluated for the deletion mutants. Figure 28 depicts the Congo red binding of solutions of BAP with varying molar ratios of the three truncated forms of the HisHSP20 protein.

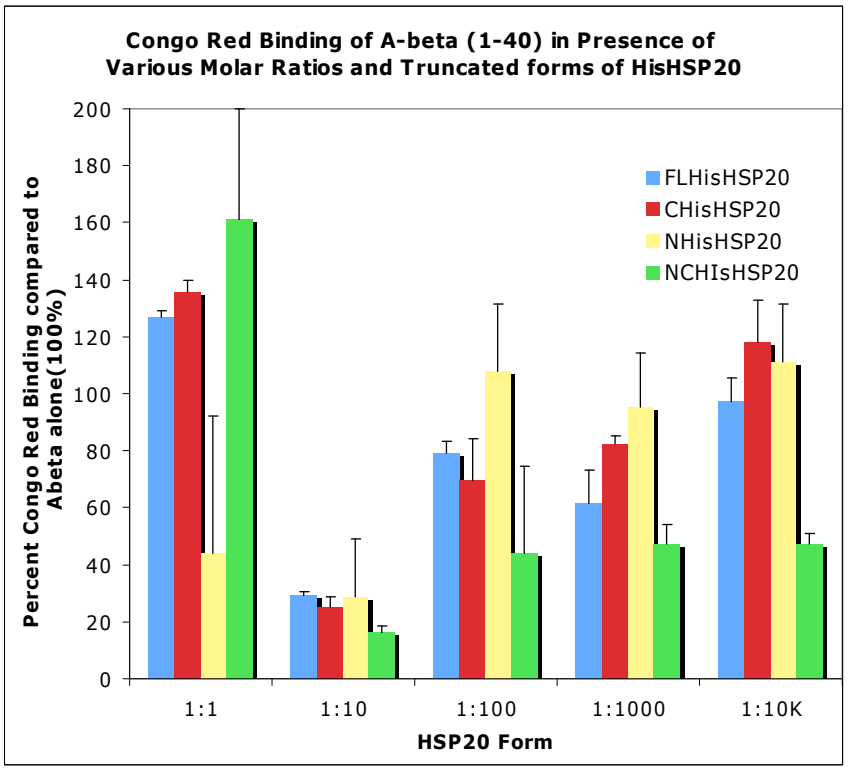

Figure 28 Inhibition of amyloid fibril formation by HisHSP20 forms. Samples of $A_{\beta(1-40)}$ (50 µM) were incubated at room temperature for 24 hours alone or in the presence of different amounts of HisHSP20 or deletion mutants of HSP20. Molar ratios of HSP20 forms to $A\beta_{(1-40)}$ are indicated on x axis. Samples were analyzed by Congo red binding as described in Chapter II. Congo red binding was used to calculate amount of fibrils formed using equation 1. Amount of fibrils formed in each sample was compared to amount of fibrils in a sample of $A\beta_{(1-40)}$ alone. The percentage of fibrils compared to that of the $A\beta_{(1-40)}$ standard is plotted on the y-axis for each molar ratio. Error bars are 1 SEM. n=3 for each molar ratio.

Again, for comparison, the full length results were included in the figure. The only molar ratio that showed a statistically different Congo red binding result is the 1:10 molar ratio of HSP20 to BAP. A one-way ANOVA at the 95% confidence interval resulted in a p-value of <0.05 when comparing the 1:10 molar ratio of all protein forms to BAP alone. Thus, the inhibitory activity of HSP20 against amyloid fibril formation is conserved despite deletion the N and C termini.

Summary and Discussion

It was not clear what roles if any the 50 amino acids in the N-terminus and the 11 amino acids of the C-terminus of HSP20 played. Others have analyzed the equivalent regions of other α-crystallins and seen that these regions are crucial for multimerization. Some have shown that these regions are also important for the function of the protein in inhibition of aggregation of partially unfolded proteins (*5, 76*). Thus it seems that these regions differ in their importance and function from one α-crystallin to the next. It was important to establish the roles of these domains within the activities and multimerization of HSP20. Deletion mutants were created based on sequence alignments with a well-characterized α-crystallin (*5*). Laksanalamai et al. reported that the sHSP isolated from the extremophile *P. furiosus* exhibited a wide range of multimeric species similar to our findings for HSP20 (*5*).

The authors created deletion mutants based on a visual analysis of the crystal structure of the *M. jannaschii* HSP16.5. They reasoned that the C-terminal 12 amino acids of *M. jannaschii* were responsible for the interdimeric contacts during assembly of the monomers into oligomers. Upon deletion of both the C-terminal 12 amino acids and

the N-terminal 52 amino acids, the authors reported a loss of all quaternary structure above a dimer (*5*).

The authors reported a diminished protection against thermally-induced cell death of *E. coli* cells producing the truncated form of the sHSP compared to cells producing the full-length protein. Laksanalamai concludes that the C-terminus is responsible for subunit assembly and that multimerization is crucial for function as the deletion mutant that did not form large multimers showed decreased activity against thermally-induced cell death. They also concluded that the N-terminal region is not needed for multimeric assembly (*5*). However, in that publication, there were no published results for a form of the *P. furiosus* HSP with the C –terminal amino acids corresponding to the oligomerization domain deleted (*5*)

A primary sequence alignment of HSP20 with the sHSP from *P. furiosus* revealed regions that corresponded to the domains attributed to multimer assembly identified by Laksanalamai (*5*). However, when these deletions were made in HSP20, the effects on multimerization and activity were different than those observed by Laksanalamai and Merk (αA-crystallin from rat) (*76*). In the case of HSP20, the multimeric population was altered when either the N-terminal or C-terminal domain was deleted. A much larger percentage of the protein existed as dimer (up to 70% as evidenced by SEC in Figure 25), but higher order complexes still existed (as shown by the sedimentation velocity experiment in Figure 26 and the western blot in Figure 22) especially for the C-terminal deletion mutant. The authors of the study on *P. furiosus* concluded that the N-terminal region was not necessary for multimeric assembly as polydisperse forms were still visible after glutaraldehyde cross linking of the N-terminal

deletion mutant (*5*). However, we have shown that a deletion of the 50 amino acids from the N-terminus of HSP20 results in a significantly reduced amount of multimeric assembly. The authors of the previous study did not test a form of the protein with only the C-terminal domain deleted. Here, we report on such a deletion mutant. It was shown that deleting the eleven C-terminal amino acids of HSP20 markedly reduces, but does not eliminate, multimeric forms of the protein. The double deletion (NCHisHSP20) still shows the presence of multimeric forms as evidenced in the sedimentation velocity experiment (Figure 26), but shows even less multimerization than that of the C-terminal deletion. The glutaraldehyde cross linking performed on the *P. furiosus* sHSP N-terminal deletion mutant resulted in an altered multimeric profile, but still showed multimers larger than dimer (*5*). In the case of HSP20, nothing larger than a dimer formed after cross-linking the N-terminal deletion mutants.

Others have reported that the N-terminal region of the sHSP's is generally unstructured. Thus, the deletion of the N-terminal fifty amino acids has likely resulted in decreased solubility of the protein. In fact, it was found that during the purification process the N-terminal deletion mutants were less stable when stored at 4°C over a period of days as the samples became turbid (unpublished observation). There was more protein at the bottom of the sedimentation velocity gradient for the N-terminal deletion mutants (Figure 26). This likely corresponds to aggregation of the protein caused by decreased solubility. Another indication of this lack of structure in the N-terminus is revealed in the CD spectra of the deletion mutants. All three mutants are very stable over the temperature range tested (5-95°C) just as the full-length protein behaved (Figure 10). The spectra of CHisHSP20 are very similar to those for the full-length

form. But the N-terminal deletion mutants have a different set of spectra (Figure 21). These spectra are shifted to the region corresponding to beta sheet and away from the region typical of unstructured proteins. This correlates quite well with the hypothesis that the N-terminus of HSP20 is largely unstructured. The secondary structure prediction software used in Figure 8 attributed very little secondary structure to the N-terminus of HSP20. Thus, when this unstructured region is deleted, the strong beta sheet signal generated as a result of the α-crystallin domain is no longer masked by the signal of the unstructured N-terminus and the spectra appears to shift to a more beta-sheet-like spectrum.

Despite deleting up to 35% of the protein (in the case of NCHisHSP20) and altering the multimeric state, the truncated forms displayed an identical activity against both thermal denaturation (Figure 27) of ADH and amyloid formation of BAP (Figure 28). In the case of the rat αA-crystallin studied by Merck et al. (*76*), a deletion of the multimeric domains not only causes arrest of multimeric assembly at the dimeric form, it also destroys the aggregation protection observed for the protein. Laksanalamai reported the double deletion of the two termini of the *P. furiosus* sHSP resulted in a greatly reduced viability of cells expressing the truncated form while incubating at elevated temperatures as opposed to cells expressing the full length version (*5*).

Though multimeric assembly is quite divergent among sHSP's, the dimer is always obsreved. This has been shown to be a result of interactions between two α-crystallin domains of two separate monomers (*6*). The larger quaternary structures vary between sHSP's with some showing a monodisperse population while others display a polydisperse one (*5, 6, 14*). Some disassemble at elevated temperatures (*6*). The work

in this dissertation shows that under the testing conditions used above, multimeric assembly has no bearing on the inhibition of aggregation of proteins by HisHSP20. However, the dimeric form of the protein is still seen. We are left to conclude that the α-crystallin domain is the source of this inhibition of aggregation. This is of great interest because the role of multimerization of α-crystallin sHSP's in function has been a central question in the field. This ability to form large dynamic structures may serve a purpose *in vivo* not observed in these experiments.

CHAPTER V

DISCUSSION AND CONCLUSIONS

An organisms ability to survive is based largely on its ability to adapt to environmental changes. The protein complement of a cell can be altered greatly due to relatively slight changes in the host's environment. This coupled with the spectrum of possible folds an individual protein can attain creates a formidable challenge for the life of the host. Organisms have developed many tools to assist them in surviving in an ever-changing environment such as the heat shock proteins. Within these groups of proteins are the α-crystallins. This diverse group has a common α-crystallin domain and often forms multimers. They function in chaperoning partially-unfolded proteins and preventing interactions with other proteins that might lead to aggregation and eventual loss of function.

Here, we investigate a novel protein isolated from *Babesia bovis* that shares homology with the α-crystallin family of sHSP's. HSP20 forms multimeric complexes from a single type of monomer as is the case for members of the α-crystallins (Figures 12-16). It has been shown here that HSP20 inhibits the aggregation of alcohol dehydrogenase at elevated temperatures at stoichiometric levels (Figures17 and 18). Finally, it has been shown to inhibit amyloid fibril formation at a sub-stoichiometric level, but not at an equimolar ratio (Figure 19).

Though sequence homology is limited, the predicted secondary structure for HSP20 is very similar to other sHSP's studied as shown in Figure 8. The region of greatest similarity is found to be within the proposed α-crystallin domain of the protein. Also, there are conserved residues within the sequence of HSP20 that correspond to

those residues found to be crucial to the function of other α-crystallins. HSP20 often forms large multimers in solution that are visible even when using SDS PAGE. In the case of HSP20, these multimeric species are a broad polydisperse group of multimers. Some α-crystallin sHSP's form discrete populations of multimers such as HSP16.5 from *M. jannaschii* (*14*),while others form a range of multimeric species under a given set of solution conditions such as the HSP fro *P.furiosus* studied by Laksanalamai et al (*5*).

Through sequence alignments and crystal structures, others have proposed models of α-crystallin multimeric assembly. Generally, the α-crystallin domain itself is thought to be involved in dimer formation, while the N and C termini are thought to be involved in higher-order assembly (*6, 14*). Deletion mutants of HSP20 were generated in an effort to gain a better understanding of its multimeric assembly. Using SEC, it was found that the capability of HSP20 to oligomerize was altered when the C-terminal 11 amino acids were deleted. The N-terminal domain has been shown to play a varying role in the multimerization of α-crystallins. It was observed by van Montfort through analysis of the x-ray crystal structure of HSP16.9 from wheat that the N-terminus of one monomer in a dimer was unstructured while the amino region of the other monomer was structured and found to be interacting with another monomer of a different dimer and was thus contributing to the stability of a large multimeric form of the protein (*6*). In the case of Laksanalamai, the N terminus of the sHSP from *P. furiosus* was shown to have little effect on multimerization (*5*) while Merck et al. showed that deletion of the N-terminus resulted in only dimer formation and a loss of aggregation protection activity in an α-crystallin isolated from rats (*32, 76*). A deletion of the first 50 amino acids of HSP20 did alter the multimeric nature of the protein but had no affect on its chaperone

activity. In Chapter IV, the proportion of NHisHSP20 multimeric forms observed at equilibrium are dramatically reduced as evidenced by various separation techniques such as SEC and electrophoresis (Figures 22-26). However, from the techniques used above, it is not clear if the same interactions between full-length monomers are preserved in the truncated forms.

As mentioned earlier, the C-terminus is thought to be responsible for interdimeric contacts, which would result in a multimeric intermediate. However, in the case if HSP20, we have shown that deletion of the N-terminus also results in the loss of this intermediate multimer as it was absent from the cross-linked sample separated by SEC under denaturing conditions (Figure 24). Thus, we propose that the N-terminus is crucial for multimeric assembly of HSP20 as well. This activity may be direct in the case of the N-terminus acting as a recruitment domain for smaller species (monomers and dimers) allowing these species to interact and align is a way that resulted in proper C-terminal contacts. This phenomenon could also be an indirect effect in that the structure of the protein was altered when the N-terminus was absent and thus the proper orientation to form multimers was attained. Finally, the N-terminus could simply be affecting the solubility of the protein. Certainly, it was observed that over time at a low temperature (4°C) the protein aggregated and fell out of solution. This is also observed in velocity sedimentation analysis in glycerol gradients. In the case of the N-terminal deletions, a larger fraction of the protein applied to the gradient was present at the bottom of the gradient suggesting aggregation during the course of the separation (which was performed at 4°C for 48 hours and is shown in Figure 26). Therefore, if the N-terminus is responsible for solubility of the protein, its absence could preclude the

formation of ordered multimers simply by disallowing proper folding and interactions to occur under the solution conditions. The phenomenon of the N-terminus playing a large role in the multimeric assembly of a sHSP is not without precedent. Leroux et al. showed that the N-terminal domain of HSP 16.2 from *C. elegans* was needed to form multimers larger than a dimer (*8*) and Merck showed loss of both oligomeric assembly and chaperone function resulting from a deletion of the N-terminus of their sHSP from rat (*32, 76*). A model which encompasses our observations of multimeric assembly is presented in Figure 29.

It has been shown that HisHSP20 inhibits the aggregation of ADH in solution at elevated temperatures, as many others have shown for other members of the α-crystallin family(*1, 11*). The greatest protection against thermally-induced aggregation of ADH was seen when equimolar amounts of HisHSP20 were present. This is in agreement with the observations of Horwitz and others with respect to protection against thermally induced aggregation by α-crystallins. Interestingly enough, the deletion mutants have no discernable effect on this activity. The three deletion mutants are equally capable of inhibiting aggregation of ADH under the conditions tested and are just as effective as the full-length version of HisHSP20 (Figure 27). Thus, it is likely that the α-crystallin domain is necessary and sufficient to maintain this activity.

The amyloidoses have garnered much attention of late. Researchers are actively investigating several methods of dealing with this devastating class of diseases. There has been a great deal of focus on the mechanism of amyloid fibril formation and how to

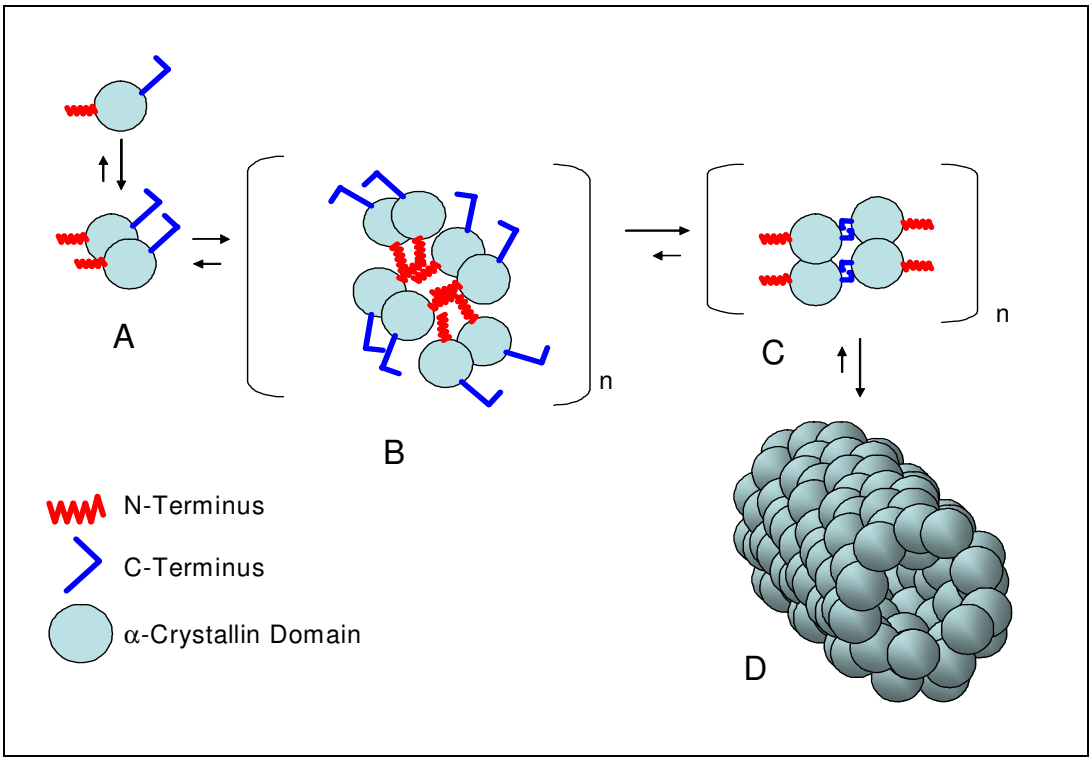

Figure 29 Model of possible oligomerization pathway of HSP20. A stable dimer is formed through interaction between α-crystallin domains (A) N-terminal domains could act as recruiting factors bringing dimers in closer proximity and proper alignment(B) for stable intermediate formation(C) leading to superstructure formation (D).

prevent it. Many research efforts have resulted in molecules that can inhibit amyloid fibril formation in vitro at equimolar ratios (*77-79*). Pallito et al. showed that a small peptide can inhibit fibril formation (*79*). Others have shown varied results with respect to α-crystallins' effectiveness against amyloid formation and toxicity in vitro (*22, 34-36, 79*). Santhoshkumar et al. developed a 19 amino acid peptide based on a portion of the α-crystallin domain that inhibits fibril formation but only at equimolar concentrations of

the fibril forming protein/peptide(*80*). Here, we report on a protein that can inhibit amyloid fibril formation of the Beta Amyloid Peptide and does so at a substoichiometric ratio. Lee and Carson (*27*) reported on the activity of this protein in the inhibition of amyloid fibril formation by the $A\beta_{(1-40)}$ peptide over a wide concentration range corresponding to molar ratios of 1:1000 to 1:100000 of HIsHSP20 to Aβ. It was reported in that same publication that the toxicity of Aβ towards neuronal cells in culture was reduced when HisHSP20 was present at these levels.

We report in Chapters III and IV that HisHSP20 and the three truncated forms can inhibit amyloid fibril formation of 50 μM $A\beta_{(1-40)}$ at a molar ratio of 1:10. Perhaps what is most impressive is the fact that despite deleting up to 35% of the protein, the specific activity of amyloid inhibition is unaffected under the conditions tested. Though the concentration range of HSP20 where protection is seen is different from the earlier work of Lee and Carson, the trend of protection at a substoichiometric level is still seen.

Also in this study, it was seen that at a molar ratio of 1:1 of HisHSP20 to Aβ, no protection was seen and in most cases, amyloid formation was greater when an equimolar amount of HisHSP20 was present (Figure 28). This trend was seen in Lee and Carson's earlier work in that as concentration of HisHSP20 increased (i.e. the molar ratio increased towards 1:1), the protection lessened. Therefore, we propose that the active form of HisHSP20 protein is interacting with a multimeric intermediate of Aβ. Because the multimeric form of HisHSP20 likely changes with its concentration, we conclude that at higher concentrations, the protein forms a multimer that does not allow productive interaction with Aβ intermediates. This is likely a result of accessible active

sites being blocked when HSP20 in in larger multimeric assemblies. Our results suggest the amount of active form of HSP20 was not altered by the changes in multimeric assembly introduced by the deletion mutants as the most effective molar ratio remains unchanged after the deletions.

The potential of HisHSP20 as an inhibitor of undesirable protein aggregation merits further study of this protein. Because the multimeric nature was altered but not abolished by the deletions constructed in the previous chapters, further study through site specific deletions of the protein around the α-crystallin domain should be performed in an effort to produce a form only capable of dimerization. The activity of this form should then be tested as described above. More structural knowledge of HSP20 would give researchers more information on potential models for inhibition of aggregation. An X-ray crystal structure of HSP20 does not exist but is currently underway. This will prove invaluable to understanding the mechanism by which HSP20 inhibits aggregation as few α-crystallins have been crystallized.

Santhoshkumar et al. described the peptide they used to inhibit amyloid fibril formation as "mini-α-crystallin". This peptide of 19 amino acids is based on a small portion of the α-crystallin domain (*80*). There is a possibility that such a small region from HSP20 could inhibit amyloidogenesis or other protein aggregation. Extensive studies have been performed by others on crucial residues of other α-crystallins (such as Arginine 120 in human αB-crystallin) (*6, 10*). Point mutational analysis of the corresponding residues in HSP20 should also be performed to determine the importance of the residues to the specific activities observed in HSP20.

Many proteins have been shown to form amyloid such as human apolipoprotein C II (apoC2) (*34*). Hatters et al. showed that α-crystallin isolated from bovine eye lenses inhibited amyloid fibril formation by apoC2 at substoichiometric amounts. The ability of HSP20 to inhibit amyloidogenesis of other proteins should be evaluated. The use of the "amyloid-specific dyes" Congo red and thioflavin T is a relatively simple and indirect method of analyzing amyloid fibril formation. The specificity and quantitative nature of these dyes is the subject of debate (*81*). To gain a better understanding of how HSP20 is interacting with amyloid precursors, other methods such as mass spectrometry and circular dichroism should be employed in an effort to study interactions between substrate and HSP20 over time. Finally, an animal model of an amyloidosis should be used in testing the efficacy of HSP20 against fibril formation in an *in vivo* setting. Research by Lee and Carson show that HisHSP20 is capable of decreasing cell death of neuronal cells in culture when exposed to $A\beta_{(1\text{-}40)}$ (*27*).

From a therapeutic standpoint, HSP20 holds a large potential. The fact that the protein inhibits amyloidogenesis in sub-stoichiometric amount is desirable as this means a much lower dosage to the patient. Also, there is the possibility that even more of the protein can be deleted without an apparent loss of function. A smaller protein would likely have fewer interactions with the host systems. As we learn more about its structure, at the very least, HSP20 can serve as a model in designing and constructing more effective treatments against amyloidogenesis. In a more general application, HSP20 is a very good candidate for acting as a preservative element for molecules that aggregate in solution or have short shelf lives such as restriction endonucleases and other enzymes.

In conclusion, we present an interesting and unique protein isolated from a protozoan erythrocyte parasite *Babesia bovis*. HSP20 exhibits many similarities to members of the α-crystallin family in both structure and activities and it is proposed here that the protein is indeed a small heat shock protein and should be classified as an α-crystallin. The protein has an α-crystallin domain identified by sequence homology with known α-crystallins. HSP20 exists as a polydisperse population of multimeric species in solution. The protein was shown to inhibit thermally induced aggregation of ADH in solution and to inhibit amyloidogenesis of the $A\beta_{(1-40)}$ peptide. Deletions were made in the regions of the protein thought to be responsible for multimerization resulting in a dramatic reduction in multimeric species. The deletion mutants constructed were designed as to not affect the α-crystallin domain in an effort to only affect multimerization and not affect activity. The deletion mutants exhibited the same levels of inhibition of aggregation of proteins as the full-length form of the protein.

REFERENCES

(1) Sun, Y., and MacRae, T. H. (2005) Small heat shock proteins: molecular structure and chaperone function. *Cell Mol Life Sci 62*, 2460-76.

(2) Hartl, F. U., and Hayer-Hartl, M. (2002) Molecular chaperones in the cytosol: from nascent chain to folded protein. *Science 295*, 1852-8.

(3) van den, I. P., Norman, D. G., and Quinlan, R. A. (1999) Molecular chaperones: small heat shock proteins in the limelight. *Curr Biol 9*, R103-5.

(4) Ehrnsperger, M., Lilie, H., Gaestel, M., and Buchner, J. (1999) The dynamics of Hsp25 quaternary structure. Structure and function of different oligomeric species. *J Biol Chem 274*, 14867-74.

(5) Laksanalamai, P., Jiemjit, A., Bu, Z., Maeder, D. L., and Robb, F. T. (2003) Multi-subunit assembly of the *Pyrococcus furiosus* small heat shock protein is essential for cellular protection at high temperature. *Extremophiles 7*, 79-83.

(6) van Montfort, R. L., Basha, E., Friedrich, K. L., Slingsby, C., and Vierling, E. (2001) Crystal structure and assembly of a eukaryotic small heat shock protein. *Nat Struct Biol 8*, 1025-30.

(7) Lee, J. S., Satoh, T., Shinoda, H., Samejima, T., Wu, S. H., and Chiou, S. H. (1997) Effect of heat-induced structural perturbation of secondary and tertiary structures on the chaperone activity of alpha-crystallin. *Biochem Biophys Res Commun 237*, 277-82.

(8) Leroux, M., Melki, R., Gordon, B., Batelier, G., and Candido, E. (1997) Structure-function studies on small heat shock protein oligomeric assembly and interaction with unfolded polypeptides. *J Biol Chem 272*, 24646-56.

(9) MacRae, T. H. (2000) Structure and function of small heat shock/alpha-crystallin proteins: established concepts and emerging ideas. *Cell Mol Life Sci 57*, 899-913.

(10) Horwitz, J. (2000) The function of alpha-crystallin in vision. *Semin Cell Dev Biol 11*, 53-60.

(11) Horwitz, J. (1992) Alpha-crystallin can function as a molecular chaperone. *Proc Natl Acad Sci U.S.A. 89*, 10449-53.

(12) Rao, C. M., Raman, B., Ramakrishna, T., Rajaraman, K., Ghosh, D., Datta, S., Trivedi, V. D., and Sukhaswami, M. B. (1998) Structural perturbation of alpha-crystallin and its chaperone-like activity. *Int J Biol Macromol 22*, 271-81.

(13) Kim, D. R., Lee, I., Ha, S. C., and Kim, K. K. (2003) Activation mechanism of HSP16.5 from *Methanococcus jannaschii*. *Biochem Biophys Res Commun 307*, 991-8.

(14) Kim, K. K., Kim, R., and Kim, S. H. (1998) Crystal structure of a small heat-shock protein. *Nature 394*, 595-9.

(15) Kim, K. K., Yokota, H., Santoso, S., Lerner, D., Kim, R., and Kim, S. H. (1998) Purification, crystallization, and preliminary X-ray crystallographic data analysis of small heat shock protein homolog from *Methanococcus jannaschii*, a hyperthermophile. *J Struct Biol 121*, 76-80.

(16) Kim, R., Kim, K. K., Yokota, H., and Kim, S. H. (1998) Small heat shock protein of *Methanococcus jannaschii*, a hyperthermophile. *Proc Natl Acad Sci U.S.A. 95*, 9129-33.

(17) Kim, R., Lai, L., Lee, H. H., Cheong, G. W., Kim, K. K., Wu, Z., Yokota, H., Marqusee, S., and Kim, S. H. (2003) On the mechanism of chaperone activity of

the small heat-shock protein of *Methanococcus jannaschii*. *Proc Natl Acad Sci U.S.A. 100*, 8151-5.

(18) Sipe, J. D., and Cohen, A. S. (2000) Review: history of the amyloid fibril. *J Struct Biol 130*, 88-98.

(19) Harper, J. D., and Lansbury, P. T., Jr. (1997) Models of amyloid seeding in Alzheimer's disease and scrapie: mechanistic truths and physiological consequences of the time-dependent solubility of amyloid proteins. *Annu Rev Biochem 66*, 385-407.

(20) Serio, T. R., Cashikar, A. G., Kowal, A. S., Sawicki, G. J., Moslehi, J. J., Serpell, L., Arnsdorf, M. F., and Lindquist, S. L. (2000) Nucleated conformational conversion and the replication of conformational information by a prion determinant. *Science 289*, 1317-21.

(21) Rymer, D. L., and Good, T. A. (2001) The role of G protein activation in the toxicity of amyloidogenic Abeta-(1-40), Abeta-(25-35), and bovine calcitonin. *J Biol Chem 276*, 2523-30.

(22) Kudva, Y. C., Hiddinga, H. J., Butler, P. C., Mueske, C. S., and Eberhardt, N. L. (1997) Small heat shock proteins inhibit in vitro A beta(1-42) amyloidogenesis. *FEBS Lett 416*, 117-21.

(23) Calne, D. B. (1994) *Neurodegenerative Diseases*, 1st ed., W.B. Saunders Company, Philadelphia.

(24) Isacson, O., Seo, H., Lin, L., Albeck, D., and Granholm, A. C. (2002) Alzheimer's disease and Down's syndrome: roles of APP, trophic factors and ACh. *Trends Neurosci 25*, 79-84.

(25) Perez, N., Sugar, J., Charya, S., Johnson, G., Merril, C., Bierer, L., Perl, D., Haroutunian, V., and Wallace, W. (1991) Increased synthesis and accumulation of heat shock 70 proteins in Alzheimer's disease. *Brain Res Mol Brain Res 11*, 249-54.

(26) Renkawek, K., Voorter, C. E., Bosman, G. J., van Workum, F. P., and de Jong, W. W. (1994) Expression of alpha B-crystallin in Alzheimer's disease. *Acta Neuropathol (Berl) 87*, 155-60.

(27) Lee, S., Carson, K., Rice-Ficht, A., and Good, T. (2005) Hsp20, a novel alpha-crystallin, prevents Abeta fibril formation and toxicity. *Protein Sci 14*, 593-601.

(28) Stege, G. J., Renkawek, K., Overkamp, P. S., Verschuure, P., van Rijk, A. F., Reijnen-Aalbers, A., Boelens, W. C., Bosman, G. J., and de Jong, W. W. (1999) The molecular chaperone alphaB-crystallin enhances amyloid beta neurotoxicity. *Biochem Biophys Res Commun 262*, 152-6.

(29) Noble, E., and Noble, G. (1982) *Parasitology:The Biology of Animal Parasites* 5th ed., Lea & Febiger, Philadelphia.

(30) Schmidt, G., and Roberts, L. (1985) *Foundations of Parasitology*, 3rd ed., Times Mirror/Mosby College Publishing, St. Louis.

(31) Brown, W. C., Ruef, B. J., Norimine, J., Kegerreis, K. A., Suarez, C. E., Conley, P. G., Stich, R. W., Carson, K. H., and Rice-Ficht, A. C. (2001) A novel 20-kilodalton protein conserved in *Babesia bovis* and *B. bigemina* stimulates memory CD4(+) T lymphocyte responses in B. bovis-immune cattle. *Mol Biochem Parasitol 118*, 97-109.

(32) Merck, K. B., Horwitz, J., Kersten, M., Overkamp, P., Gaestel, M., Bloemendal, H., and de Jong, W. W. (1993) Comparison of the homologous carboxy-terminal domain and tail of alpha-crystallin and small heat shock protein. *Mol Biol Rep 18*, 209-15.

(33) Salerno, J. C., Eifert, C. L., Salerno, K. M., and Koretz, J. F. (2003) Structural diversity in the small heat shock protein superfamily: control of aggregation by the N-terminal region. *Protein Eng 16*, 847-51.

(34) Hatters, D. M., Lindner, R. A., Carver, J. A., and Howlett, G. J. (2001) The molecular chaperone, alpha-crystallin, inhibits amyloid formation by apolipoprotein C-II. *J Biol Chem 276*, 33755-61.

(35) Raman, B., Ban, T., Sakai, M., Pasta, S. Y., Ramakrishna, T., Naiki, H., Goto, Y., and Rao Ch, M. (2005) AlphaB-crystallin, a small heat-shock protein, prevents the amyloid fibril growth of an amyloid beta-peptide and beta2-microglobulin. *Biochem J 392*, 573-81.

(36) Rekas, A., Adda, C. G., Andrew Aquilina, J., Barnham, K. J., Sunde, M., Galatis, D., Williamson, N. A., Masters, C. L., Anders, R. F., Robinson, C. V., Cappai, R., and Carver, J. A. (2004) Interaction of the molecular chaperone alphaB-crystallin with alpha-synuclein: effects on amyloid fibril formation and chaperone activity. *J Mol Biol 340*, 1167-83.

(37) Carrington, J. C., and Dougherty, W. G. (1988) A viral cleavage site cassette: identification of amino acid sequences required for tobacco etch virus polyprotein processing. *Proc Natl Acad Sci U.S.A. 85*, 3391-5.

(38) Klunk, W. E., Jacob, R. F., and Mason, R. P. (1999) Quantifying amyloid beta-peptide (Abeta) aggregation using the Congo red-Abeta (CR-abeta) spectrophotometric assay. *Anal Biochem 266*, 66-76.

(39) Gasteiger E., H. C., Gattiker A., Duvaud S., Wilkins M.R., Appel R.D., Bairoch A (2005) *Protein Identification and Analysis Tools on the ExPASy Server*, Humana Press, Totowa, NJ.

(40) Pace, C. N., Vajdos, F., Fee, L., Grimsley, G., and Gray, T. (1995) How to measure and predict the molar absorption coefficient of a protein. *Protein Sci 4*, 2411-23.

(41) Falquet, L., Pagni, M., Bucher, P., Hulo, N., Sigrist, C. J., Hofmann, K., and Bairoch, A. (2002) The PROSITE database, its status in 2002. *Nucleic Acids Res 30*, 235-8.

(42) Jones, D. T. (1999) Protein secondary structure prediction based on position-specific scoring matrices. *J Mol Biol 292*, 195-202.

(43) McGuffin, L. J., Bryson, K., and Jones, D. T. (2000) The PSIPRED protein structure prediction server. *Bioinformatics 16*, 404-5.

(44) Creighton, T. (1993) *Proteins: Structures and Molecular Properties*, 2 ed., W.H. Freeman and Company, New York.

(45) Haley, D. A., Bova, M. P., Huang, Q. L., McHaourab, H. S., and Stewart, P. L. (2000) Small heat-shock protein structures reveal a continuum from symmetric to variable assemblies. *J Mol Biol 298*, 261-72.

(46) Haslbeck, M., Braun, N., Stromer, T., Richter, B., Model, N., Weinkauf, S., and Buchner, J. (2004) Hsp42 is the general small heat shock protein in the cytosol of *Saccharomyces cerevisiae*. *Embo J 23*, 638-49.

(47) Rogalla, T., Ehrnsperger, M., Preville, X., Kotlyarov, A., Lutsch, G., Ducasse, C., Paul, C., Wieske, M., Arrigo, A. P., Buchner, J., and Gaestel, M. (1999) Regulation of Hsp27 oligomerization, chaperone function, and protective activity against oxidative stress/tumor necrosis factor alpha by phosphorylation. *J Biol Chem 274*, 18947-56.

(48) Biswas, A., Miller, A., Oya-Ito, T., Santhoshkumar, P., Bhat, M., and Nagaraj, R. (2006) Effect of site-directed mutagenesis of methylglyoxal-modifiable arginine residues on the structure and chaperone function of human alphaA-crystallin. *Biochemistry 45*, 4569-4577.

(49) Chang, Z., Primm, T., Jakana, J., Lee, I., Serysheva, I., Chiu, W., Gilbert, H., and Quiocho, F. (1996) *Mycobacterium tuberculosis* 16-kDa antigen (Hsp16.3) functions as an oligomeric structure in vitro to suppress thermal aggregation. *J Biol Chem 271*, 7218-23.

(50) Chowdary, T., Raman, B., Ramakrishna, T., and Rao, C. (2004) Mammalian Hsp22 is a heat-inducible small heat-shock protein with chaperone-like activity. *Biochem J 381*, 379-87.

(51) Ding, L., and Candido, E. (2000) HSP25, a small heat shock protein associated with dense bodies and M-lines of body wall muscle in *Caenorhabditis elegans*. *J Biol Chem 275*, 9510-7.

(52) Ghosh, J., Estrada, M., and Clark, J. (2005) Interactive domains for chaperone activity in the small heat shock protein, human alphaB crystallin. *Biochemistry 44*, 14854-69.

(53) Jakob, U., Gaestel, M., Engel, K., and Buchner, J. (1993) Small heat shock proteins are molecular chaperones. *J Biol Chem 268*, 1517-20.

(54) Liang, P., Amons, R., Macrae, T., and Clegg, J. (1997) Purification, structure and in vitro molecular-chaperone activity of *Artemia* p26, a small heat-shock/alpha-crystallin protein. *Eur J Biochem 243*, 225-32.

(55) Muchowski, P., and Clark, J. (1998) ATP-enhanced molecular chaperone functions of the small heat shock protein human alphaB crystallin. *Proc Natl Acad Sci U.S.A. 95*, 1004-9.

(56) Rajaraman, K., Raman, B., Ramakrishna, T., and Rao, C. (2001) Interaction of human recombinant alphaA- and alphaB-crystallins with early and late unfolding intermediates of citrate synthase on its thermal denaturation. *FEBS Lett 497*, 118-23.

(57) Roy, S., Hiyama, T., and Nakamoto, H. (1999) Purification and characterization of the 16-kDa heat-shock-responsive protein from the thermophilic cyanobacterium *Synechococcus vulcanus*, which is an alpha-crystallin-related, small heat shock protein. *Eur J Biochem 262*, 406-16.

(58) Santhoshkumar, P., and Sharma, K. (2001) Phe71 is essential for chaperone-like function in alpha A-crystallin. *J Biol Chem 276*, 47094-9.

(59) Santhoshkumar, P., and Sharma, K. (2001) Analysis of alpha-crystallin chaperone function using restriction enzymes and citrate synthase. *Mol Vis 7*, 172-7.

(60) Smykal, P., Masin, J., Hrdy, I., Konopasek, I., and Zarsky, V. (2000) Chaperone activity of tobacco HSP18, a small heat-shock protein, is inhibited by ATP. *Plant J 23*, 703-13.

(61) Studer, S., Obrist, M., Lentze, N., and Narberhaus, F. (2002) A critical motif for oligomerization and chaperone activity of bacterial alpha-heat shock proteins. *Eur J Biochem 269*, 3578-86.

(62) Valdez, M., Clark, J., Wu, G., and Muchowski, P. (2002) Functional similarities between the small heat shock proteins *Mycobacterium tuberculosis* HSP 16.3 and human alphaB-crystallin. *Eur J Biochem 269*, 1806-13.

(63) Wang, K., and Spector, A. (2000) alpha-crystallin prevents irreversible protein denaturation and acts cooperatively with other heat-shock proteins to renature the stabilized partially denatured protein in an ATP-dependent manner. *Eur J Biochem 267*, 4705-12.

(64) Lentze, N., Studer, S., and Narberhaus, F. (2003) Structural and functional defects caused by point mutations in the alpha-crystallin domain of a bacterial alpha-heat shock protein. *J Mol Biol 328*, 927-37.

(65) Mao, Q., Ke, D., Feng, X., and Chang, Z. (2001) Preheat treatment for *Mycobacterium tuberculosis* Hsp16.3: correlation between a structural phase change at 60 degrees C and a dramatic increase in chaperone-like activity. *Biochem Biophys Res Commun 284*, 942-7.

(66) Bova, M. P., McHaourab, H. S., Han, Y., and Fung, B. K. (2000) Subunit exchange of small heat shock proteins. Analysis of oligomer formation of alphaA-crystallin and Hsp27 by fluorescence resonance energy transfer and site-directed truncations. *J Biol Chem 275*, 1035-42.

(67) Eifert, C., Burgio, M. R., Bennett, P. M., Salerno, J. C., and Koretz, J. F. (2005) N-terminal control of small heat shock protein oligomerization: changes in aggregate size and chaperone-like function. *Biochim Biophys Acta 1748*, 146-56.

(68) Jiao, W., Qian, M., Li, P., Zhao, L., and Chang, Z. (2005) The essential role of the flexible termini in the temperature-responsiveness of the oligomeric state and chaperone-like activity for the polydisperse small heat shock protein IbpB from *Escherichia coli*. *J Mol Biol 347*, 871-84.

(69) Koteiche, H. A., and McHaourab, H. S. (2002) The determinants of the oligomeric structure in Hsp16.5 are encoded in the alpha-crystallin domain. *FEBS Lett 519*, 16-22.

(70) Lambert, H., Charette, S. J., Bernier, A. F., Guimond, A., and Landry, J. (1999) HSP27 multimerization mediated by phosphorylation-sensitive intermolecular interactions at the amino terminus. *J Biol Chem 274*, 9378-85.

(71) Lelj-Garolla, B., and Mauk, A. G. (2005) Self-association of a small heat shock protein. *J Mol Biol 345*, 631-42.

(72) Stromer, T., Fischer, E., Richter, K., Haslbeck, M., and Buchner, J. (2004) Analysis of the regulation of the molecular chaperone Hsp26 by temperature-induced dissociation: the N-terminal domain is important for oligomer assembly and the binding of unfolding proteins. *J Biol Chem 279*, 11222-8.

(73) Sun, Y., Mansour, M., Crack, J. A., Gass, G. L., and MacRae, T. H. (2004) Oligomerization, chaperone activity, and nuclear localization of p26, a small heat shock protein from *Artemia franciscana*. *J Biol Chem 279*, 39999-40006.

(74) Wintrode, P. L., Friedrich, K. L., Vierling, E., Smith, J. B., and Smith, D. L. (2003) Solution structure and dynamics of a heat shock protein assembly probed by hydrogen exchange and mass spectrometry. *Biochemistry 42*, 10667-73.

(75) Young, L. S., Yeh, C. H., Chen, Y. M., and Lin, C. Y. (1999) Molecular characterization of *Oryza sativa* 16.9 kDa heat shock protein. *Biochem J 344 Pt 1*, 31-8.

(76) Merck, K. B., De Haard-Hoekman, W. A., Oude Essink, B. B., Bloemendal, H., and De Jong, W. W. (1992) Expression and aggregation of recombinant alpha A-crystallin and its two domains. *Biochim Biophys Acta 1130*, 267-76.

(77) Ghanta, J., Shen, C. L., Kiessling, L. L., and Murphy, R. M. (1996) A strategy for designing inhibitors of beta-amyloid toxicity. *J Biol Chem 271*, 29525-8.

(78) Lowe, T. L., Strzelec, A., Kiessling, L. L., and Murphy, R. M. (2001) Structure-function relationships for inhibitors of beta-amyloid toxicity containing the recognition sequence KLVFF. *Biochemistry 40*, 7882-9.

(79) Pallitto, M. M., Ghanta, J., Heinzelman, P., Kiessling, L. L., and Murphy, R. M. (1999) Recognition sequence design for peptidyl modulators of beta-amyloid aggregation and toxicity. *Biochemistry 38*, 3570-8.

(80) Santhoshkumar, P., and Sharma, K. K. (2004) Inhibition of amyloid fibrillogenesis and toxicity by a peptide chaperone. *Mol Cell Biochem 267*, 147-55.

(81) Khurana, R., Uversky, V. N., Nielsen, L., and Fink, A. L. (2001) Is Congo red an amyloid-specific dye? *J Biol Chem 276*, 22715-21.

VITA

Name: Kenneth Harris Carson

Address: c/o Dr. Allison C. Rice-Ficht

440 Reynolds Medical Building

1114 TAMU, College Station, TX 77843-1114

Email address: kenneth-h-carson@neo.tamu.edu

Education: B.S., Chemistry, The University of Texas at Tyler, 1997

Ph.D., Medical Sciences, Texas A&M University, 2006

Selected Publications

Brown, W. C., Ruef, B.J., Norimini, J., Kegerreis, K., Conley, P., Stich, R.W., Carson, K, and Ficht, A.C. (2001) A Novel 20-kilodalton protein conserved in Babesia bovis and Babesia bigemina stimulates memory CD4+ T lymphocyte responses in B. bovis-immune cattle. Molecular and Biochemical Prasitology 118, 97-109.

Bahukudumbi, P., Carson, K.H., Rice-Ficht, A.C., and Andrews, M.J. (2004) On the diameter and size distributions of bovine serum albumin (BSA)-based Microspheres. Journal of Microencapsulation 21, 787-804

Lee, S., Carson, K., Rice-Ficht, A.C. and Good, T. (20005) HSP20, a novel α-crystallin, prevents Ab fibril formation and toxicity. Protein Science 14, 593-602